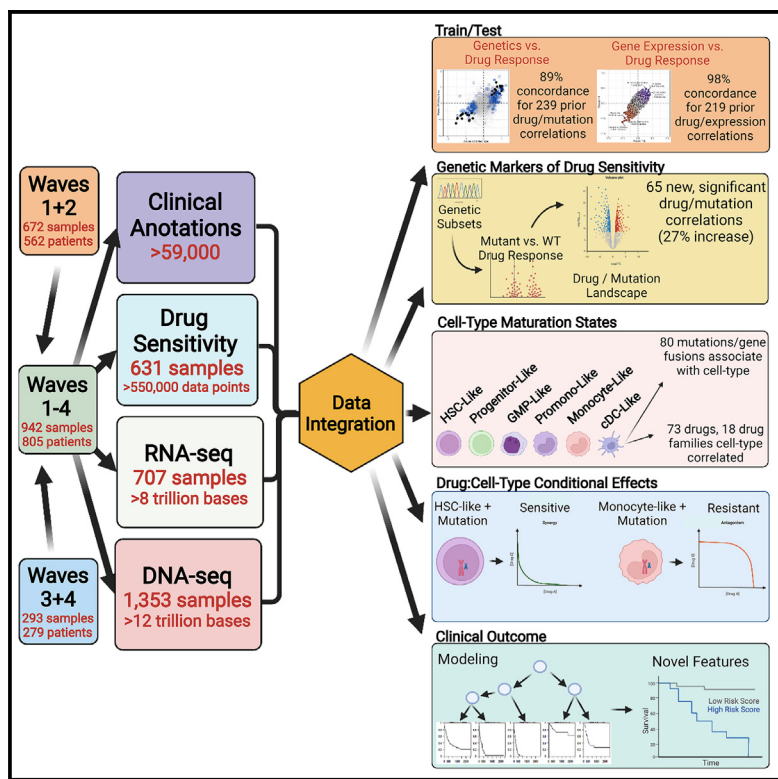


## Integrative analysis of drug response and clinical outcome in acute myeloid leukemia

### Graphical abstract



### Authors

Daniel Bottomly, Nicola Long,  
Anna Reister Schultz, ...,  
Brian J. Druker,  
Shannon K. McWeeney,  
Jeffrey W. Tyner

### Correspondence

drukerb@ohsu.edu (B.J.D.),  
mcweeney@ohsu.edu (S.K.M.),  
tynerj@ohsu.edu (J.W.T.)

### In brief

Bottomly et al. present a functional genomic resource composed of molecular, clinical, and drug response data on acute myeloid leukemia patient specimens. Through integration of all of these data, they identify genetic and cell differentiation state features that predict drug response, and they utilize modeling to identify targetable determinants of clinical outcome.

### Highlights

- Acute myeloid leukemia patient cohort with clinical, molecular, drug response data
- Validation and discovery of diverse biological features of drug response
- Broad mapping of tumor cell differentiation state affecting response to drugs
- Modeling reveals a strong and targetable determinant of clinical outcome



## Article

# Integrative analysis of drug response and clinical outcome in acute myeloid leukemia

Daniel Bottomly,<sup>1,2,31</sup> Nicola Long,<sup>2,3,31</sup> Anna Reister Schultz,<sup>2,4,31</sup> Stephen E. Kurtz,<sup>2,3,31</sup> Cristina E. Tognon,<sup>2,3,31</sup> Kara Johnson,<sup>2,3,31</sup> Melissa Abel,<sup>2,4</sup> Anupriya Agarwal,<sup>2,4,5,6</sup> Sammantha Avaylon,<sup>2,3</sup> Erik Benton,<sup>1,7</sup> Aurora Blucher,<sup>1,2</sup> Uma Borate,<sup>8</sup> Theodore P. Braun,<sup>2,3</sup> Jordana Brown,<sup>2,4</sup> Jade Bryant,<sup>2,4</sup> Russell Burke,<sup>2,3</sup> Amy Carlos,<sup>2,9</sup> Bill H. Chang,<sup>2,10</sup> Hyun Jun Cho,<sup>2,11</sup> Stephen Christy,<sup>2,3</sup> Cody Coblenz,<sup>2,3</sup> Aaron M. Cohen,<sup>1,2,7</sup> Amanda d'Almeida,<sup>2,4</sup> Rachel Cook,<sup>2,3</sup> Alexey Danilov,<sup>12</sup> Kim-Hien T. Dao,<sup>13</sup> Michie Deginn,<sup>2,3</sup> James Dibb,<sup>2,3</sup> Christopher A. Eide,<sup>2,3</sup> Isabel English,<sup>2,3</sup> Stuart Hagler,<sup>1,7</sup> Heath Harrelson,<sup>1,7</sup> Rachel Henson,<sup>2,9</sup> Hibery Ho,<sup>2,3</sup> Sunil K. Joshi,<sup>2,3</sup> Brian Junio,<sup>2,3</sup> Andy Kaempf,<sup>2,14</sup> Yoko Kosaka,<sup>2,11</sup> Ted Laderas,<sup>15</sup> Matt Lawhead,<sup>1,7</sup> Hyunjung Lee,<sup>2,4</sup> Jessica T. Leonard,<sup>2,3</sup> Chenwei Lin,<sup>2,9</sup> Evan F. Lind,<sup>2,11</sup> Selina Qiuying Liu,<sup>2,3</sup> Pierrette Lo,<sup>2,3</sup> Marc M. Loriaux,<sup>2,16</sup> Samuel Luty,<sup>2,3</sup>

(Author list continued on next page)

<sup>1</sup>Division of Bioinformatics and Computational Biology, Department of Medical Informatics and Clinical Epidemiology, Oregon Health & Science University, Portland, OR 97239, USA

<sup>2</sup>Knight Cancer Institute, Oregon Health & Science University, Portland, OR 97239, USA

<sup>3</sup>Division of Hematology & Medical Oncology, Department of Medicine, Oregon Health & Science University, Portland, OR 97239, USA

<sup>4</sup>Department of Cell, Developmental & Cancer Biology, Oregon Health & Science University, Portland, OR 97239, USA

<sup>5</sup>Department of Molecular & Medical Genetics, Oregon Health & Science University, Portland, OR 97239, USA

<sup>6</sup>Division of Oncologic Sciences, Department of Medicine, Oregon Health & Science University, Portland, OR 97239, USA

<sup>7</sup>Oregon Clinical and Translational Research Institute, Oregon Health & Science University, Portland, OR 97239, USA

<sup>8</sup>Division of Hematology, Department of Internal Medicine, James Cancer Center, Ohio State University, Columbus, OH 43210, USA

<sup>9</sup>Integrated Genomics Laboratory, Oregon Health & Science University, Portland, OR 97239, USA

<sup>10</sup>Division of Hematology and Oncology, Department of Pediatrics, Oregon Health & Science University, Portland, OR 97239, USA

<sup>11</sup>Department of Molecular Microbiology and Immunology, Oregon Health & Science University, Portland, OR 97239, USA

<sup>12</sup>Department of Hematology and Hematopoietic Stem Cell Transplant, City of Hope National Medical Center, Duarte, CA 91010, USA

<sup>13</sup>Astex Pharmaceuticals, Cambridge, CB4 0QA, UK

<sup>14</sup>Biostatistics Shared Resource, Oregon Health & Science University, Portland, OR 97239, USA

<sup>15</sup>DNA Nexus, Mountain View, CA 94040, USA

<sup>16</sup>Department of Pathology, Oregon Health & Science University, Portland, OR 97239, USA

<sup>17</sup>OHSU-PSU School of Public Health, VA Portland Health Care System, Oregon Health & Science University, Portland, OR 97239, USA

<sup>18</sup>Department of Biostatistics, St. Jude Children's Research Hospital, Memphis, TN 38105, USA

(Affiliations continued on next page)

## SUMMARY

Acute myeloid leukemia (AML) is a cancer of myeloid-lineage cells with limited therapeutic options. We previously combined *ex vivo* drug sensitivity with genomic, transcriptomic, and clinical annotations for a large cohort of AML patients, which facilitated discovery of functional genomic correlates. Here, we present a dataset that has been harmonized with our initial report to yield a cumulative cohort of 805 patients (942 specimens). We show strong cross-cohort concordance and identify features of drug response. Further, deconvoluting transcriptomic data shows that drug sensitivity is governed broadly by AML cell differentiation state, sometimes conditionally affecting other correlates of response. Finally, modeling of clinical outcome reveals a single gene, PEAR1, to be among the strongest predictors of patient survival, especially for young patients. Collectively, this report expands a large functional genomic resource, offers avenues for mechanistic exploration and drug development, and reveals tools for predicting outcome in AML.

## INTRODUCTION

Acute myeloid leukemia (AML) is characterized by neoplastic proliferation of myeloid-lineage cells. Approximately 21,000 diagnoses and 10,000 AML-related deaths are reported annually

in the United States (Jemal et al., 2010; SEER, 2021). Genetic features include 16 recurrent gene rearrangements and a plethora of unique, tumor-specific aberrations (Arber et al., 2016). In addition, ~60 genes exhibit recurrent point mutations with many thousand additional rarely mutated genes (Cancer



Julia E. Maxson,<sup>2,6</sup> Tara Macey,<sup>2,3</sup> Jacqueline Martinez,<sup>2,3</sup> Jessica Minnier,<sup>2,14,17</sup> Andrea Montebelanco,<sup>2,3</sup> Motomi Mori,<sup>18</sup> Quinlan Morrow,<sup>2,4</sup> Dylan Nelson,<sup>19</sup> Justin Ramsdill,<sup>1,7</sup> Angela Rofelty,<sup>2,4</sup> Alexandra Rogers,<sup>2,3</sup> Kyle A. Romine,<sup>2,4</sup> Peter Ryabinin,<sup>1,2</sup> Jennifer N. Saultz,<sup>2,3</sup> David A. Sampson,<sup>2,3</sup> Samantha L. Savage,<sup>2,3</sup> Robert Schuff,<sup>20</sup> Robert Searles,<sup>2,9</sup> Rebecca L. Smith,<sup>2,3</sup> Stephen E. Spurgeon,<sup>2,3</sup> Tyler Sweeney,<sup>2,3</sup> Ronan T. Swords,<sup>2,3</sup> Aashis Thapa,<sup>2,3</sup> Karina Thiel-Klare,<sup>2,3</sup> Elie Traer,<sup>2,3</sup> Jake Wagner,<sup>2,3</sup> Beth Wilmot,<sup>1,7</sup> Joelle Wolf,<sup>2,3</sup> Guanming Wu,<sup>1,2,7</sup> Amy Yates,<sup>1,7</sup> Haijiao Zhang,<sup>2,6</sup> Christopher R. Cogle,<sup>21</sup> Robert H. Collins,<sup>22</sup> Michael W. Deininger,<sup>23,24</sup> Christopher S. Hourigan,<sup>25</sup> Craig T. Jordan,<sup>26</sup> Tara L. Lin,<sup>27</sup> Micaela E. Martinez,<sup>28</sup> Rachel R. Pallapati,<sup>28</sup> Daniel A. Pollyea,<sup>26</sup> Anthony D. Pomicter,<sup>24</sup> Justin M. Watts,<sup>29</sup> Scott J. Weir,<sup>30</sup> Brian J. Druker,<sup>2,3,\*</sup> Shannon K. McWeeney,<sup>1,2,7,31,\*</sup> and Jeffrey W. Tyner<sup>2,4,31,32,\*</sup>

<sup>19</sup>High-Throughput Screening Services Laboratory, Oregon State University, Corvallis, OR 97331, USA

<sup>20</sup>Ochin Inc., Portland, OR 97228, USA

<sup>21</sup>Department of Medicine, Division of Hematology and Oncology, University of Florida, Gainesville, FL 32610, USA

<sup>22</sup>Department of Internal Medicine/ Hematology Oncology, University of Texas Southwestern Medical Center, Dallas, TX 75390-8565, USA

<sup>23</sup>Division of Hematology & Hematologic Malignancies, Department of Internal Medicine, University of Utah, Salt Lake City, UT 84112, USA

<sup>24</sup>Huntsman Cancer Institute, University of Utah, Salt Lake City, UT 84112, USA

<sup>25</sup>National Heart, Lung and Blood Institute, National Institutes of Health, Bethesda, MD 20814-1476, USA

<sup>26</sup>Division of Hematology, University of Colorado, Denver, CO 80045, USA

<sup>27</sup>Division of Hematologic Malignancies & Cellular Therapeutics, University of Kansas, Kansas City, KS 66205, USA

<sup>28</sup>Clinical Research Services, University of Miami Sylvester Comprehensive Cancer Center, Miami, FL 33136, USA

<sup>29</sup>Division of Hematology, Department of Medicine, University of Miami Sylvester Comprehensive Cancer Center, Miami, FL 33136, USA

<sup>30</sup>Department of Cancer Biology, Division of Medical Oncology, Department of Medicine, University of Kansas Medical Center, Kansas City, KS 66160, USA

<sup>31</sup>These authors contributed equally

<sup>32</sup>Lead contact

\*Correspondence: drukerb@ohsu.edu (B.J.D.), mcweeney@ohsu.edu (S.K.M.), tynerj@ohsu.edu (J.W.T.)

<https://doi.org/10.1016/j.ccel.2022.07.002>

Genome Atlas Research et al., 2013; Papaemmanuil et al., 2016; Tyner et al., 2018). Conventional chemotherapies combine anthracyclines with nucleoside analogs and a subsequent bone marrow transplant for ~20% of patients. This results in durable remission for only ~20% of patients (Pulte et al., 2016).

AML tumors also exhibit a diversity of cell phenotypes that can be aligned with differentiation states in healthy hematopoiesis. These phenotypes have been captured in classification schemes such as the French-American-British (FAB) system (Bennett et al., 1976) and from the World Health Organization (WHO) (Arber et al., 2016). Gene expression signatures from the most primitive AML cell state, leukemic stem cells (LSCs), have been shown to carry prognostic significance in AML and myelodysplastic syndromes (MDSs) (Elsayed et al., 2020; Gal et al., 2006; Gentles et al., 2010; Horibata et al., 2019; Ng et al., 2016; Wang et al., 2020). Most recently, single-cell sequencing has been employed to describe gene expression signatures that define six distinct AML tumor maturation states (Van Galen et al., 2019).

Rationally targeted therapeutics for AML include all-trans retinoic acid combined with arsenic trioxide (Huang et al., 1988; Shen et al., 1997); small-molecules targeting mutated enzymes such as fms related tyrosine kinase 3 (FLT3) (gilteritinib [Perl et al., 2019] and midostaurin [Stone et al., 2017]) or isocitrate dehydrogenase (NADP<sup>+</sup>) 1/2 (IDH1/2) (ivosidenib [DiNardo et al., 2018] and enasidenib [Stein et al., 2017]), an antibody drug conjugate targeting CD33 (gemtuzumab; Petersdorf et al., 2013), a liposomal formulation of cytarabine and daunorubicin (CPX-351; Lancet et al., 2018), and the BCL2 inhibitor, venetoclax, used in combination with hypomethylating agents (azacitidine or decitabine) (DiNardo et al., 2019). Despite these tools, drug resistance and disease relapse remain persistent problems necessitating a more complete understanding of the biological factors driving drug response.

## RESULTS

To better understand the factors governing AML drug response and clinical outcome, we developed a comprehensive platform to combine clinical, cellular, and molecular features of disease. Our complete Oregon Health & Science University (OHSU) Beat AML cohort represents sample collection and characterization over a span of 10 years with integration of *ex vivo* drug sensitivity testing, curation of clinical annotations, and DNA and RNA sequencing (RNA-seq). The data in Tyner et al. (2018) represent the first tranche of patient sample data (denoted as waves 1 + 2). Here, we provide additional longitudinal samples for waves 1 + 2, updated clinical information, as well as additional patient accrual, which represents the final two waves (waves 3 + 4). Waves 3 + 4, collected over a 2.5-year period, comprise a total of 293 specimens from 279 patients (243 patients unique to waves 3 + 4). We also provide the harmonization of these datasets together, for a cumulative cohort of 942 specimens from 805 patients, which reflects a real-world cohort of AML cases, inclusive of *de novo*, transformed, and therapy-related AML as well as cases at the point of initial diagnosis (70% of cases) and smaller numbers with relapsed or residual disease. A full listing of samples, available data, and clinical annotations are in Table S1. All somatic variant calls, gene expression counts, and drug response data can be explored and visualized through our interactive browser, Vizome ([vizome.org/aml2](http://vizome.org/aml2)). For all cohort-level analyses, only specimens from the first timepoint of each patient were used (defined in Table S1), with all remission samples excluded. A broad overview of clinical data showed comparable features between the two datasets with only a slightly lower percentage of cases with *de novo* AML in the first dataset (49% in waves 1 + 2 versus 58% in waves 3 + 4). Frequencies of the most commonly mutated genes were also equivalent between cohorts (Figure 1A). Clinical outcomes, as

measured by overall survival, of patients whose specimens were collected during the first cohort were indistinguishable from those collected during the second cohort (Figure 1B). The *ex vivo* drug sensitivity data were compared in *de novo* samples for each dataset, due to our prior observation that general drug sensitivity is reduced in secondary AML cases (Tyner et al., 2018), and showed high concordance (Figure 1C). We harmonized the RNA-seq data across the waves (Figure S1A) by re-using the parameters and reference distribution of the conditional quantile normalization (CQN) (Hansen et al., 2012) procedure applied previously. We highlight this with our prior weighted gene co-expression network analysis (WGCNA) (Zhang and Horvath, 2005) that identified 13 gene expression modules across waves 1 + 2 (Tyner et al., 2018). Part of the WGCNA methodology involves the summarization of each module by its first principal component (PC) score (termed an eigengene; Horvath and Dong, 2008). Using the parameters (e.g., means, standard deviations, and rotations) learned from waves 1 + 2, we predicted the PC scores of the waves 3 + 4 samples for each module and revealed near-complete overlap in every module with respect to range, distributions, and clustering (Figure S1B). Finally, our prior analysis included integration of *ex vivo* drug sensitivity with both mutational/cytogenetic status and gene expression to identify genomic or transcriptomic predictors of drug response. We observed strong concordance of associations between drug sensitivity and mutational status (89% concordance of waves 1 + 2 and waves 3 + 4), with nearly all associations showing a similar effect size in both the positive and negative direction (Figure 1D). In addition, we assessed correlation between gene expression (13 WGCNA module eigengenes) and drug response, revealing 98% concordance for these associations in waves 1 + 2 versus waves 3 + 4 (Figure S1C).

### Deconvoluting AML cell maturation state

We and others have observed that drug response patterns in AML are sometimes correlated with maturation state of AML tumor cells, with certain drugs exhibiting stronger efficacy against tumors with less differentiated cell state (e.g., BCL2i, cyclin dependent kinase 4/6 [CDK4/6]; Kuusankoski et al., 2020; Majumder et al., 2020; Pei et al., 2020; Romine et al., 2021; Zhang et al., 2020) and others showing better efficacy against tumors with more differentiated state (e.g., bromodomain containing 4 [BRD4/BET] i, mitogen-activated protein kinase kinase [MAPKK/MEK]i; Romine et al., 2021; White et al., 2021). Analytical approaches can facilitate the deconvolution of deep-sequencing data to infer proportions of distinct cell types (Avila Cobos et al., 2018), and single-cell sequencing technology has recently defined gene expression patterns for six distinct cell types in AML (hematopoietic stem cell [HSC]-like, progenitor-like, granulocyte-monocyte progenitor [GMP]-like, promonocyte-like, monocyte-like, and conventional dendritic cell [cDC]-like types; Van Galen et al., 2019). We summarized each of these six signatures by their PC1 scores (similar to the WGCNA eigengene). An example of the formation of the monocyte-like score is shown in Figure S2A. Comparison of the HSC-like or monocyte-like scores against FAB subtypes showed higher overall scores for the HSC-like type in the less differentiated M0–M2 samples and higher monocyte-like scores in the myelomonocytic and monocytic M4–M5 groups (Figure S2B). To understand the relationship between our WGCNA modules and

differences in cell type, we compared eigengene scores of each signature. We found WGCNA modules that correlate strongly with the more differentiated cell types ( $N = 5$ ), less differentiated cell types ( $N = 3$ ), as well as those that exhibit correlation with early- and late-stage cell types ( $N = 5$ ) (Figure 2A). Finally, we wanted to understand whether mutational or cytogenetic features showed enrichment for AML cell-type signatures. Indeed, we observed numerous significant correlations, including tumor protein 53 (TP53), bcl6 corepressor (BCOR), and splicing factor 3b subunit 1 (SF3B1) enriched for HSC-like state, nucleophosmin 1 (NPM1) enriched for promonocyte-like state, RAS correlating with monocyte-like state, and numerous other associations. Interestingly, the associations were not always compartmentalized or linear; for instance, RUNX family transcription factor 1 (RUNX1) showed strong correlation with both HSC-like (the most primitive) and cDC-like (the most differentiated), suggesting that RUNX1-mutant AML tumors may co-opt features of multiple, disparate cell maturation states (Figure 2B; for all associations see Table S2).

We next wanted to determine the breadth of drugs with response that is correlated with AML cell differentiation state and, accordingly, compared the six cell-type scores with drug response across our full panel. Overall, 73 drugs showed response that significantly correlated with at least one cell type. Hierarchical clustering of these 73 drugs revealed three main groups. One cluster contained a series of inhibitors with greater activity against HSC- and progenitor-like states and with less efficacy against the more differentiated cell types. Another cluster displayed the inverse pattern with greatest activity against the cDC- and monocyte-like states. The third cluster showed some, albeit muted, activity against both HSC-/progenitor-like and cDC-/monocyte-like states with the most resistance conferred by GMP- and promonocyte-like states (Figure 3A; for all associations see Table S3). Finally, there were two drugs, venetoclax and the histone deacetylase (HDAC) inhibitor, panobinostat, that were extreme outliers and exhibited inverse patterns of response (Figure S3A). We next wanted to understand whether any of the associations between drug response and cell-type score might be conditional on mutational or cytogenetic events. Numerous instances of significant interactions between cell-type score and mutational/cytogenetic events were identified, mostly involving the monocyte-like score (Figure 3B). For example, sorafenib is a potent inhibitor of the FLT3 receptor tyrosine kinase and exhibits significantly greater efficacy in FLT3-internal tandem duplication (ITD) mutant samples. However, inclusion of cell-type scores reveals that sorafenib shows stronger efficacy in cases with both FLT3-ITD and a high progenitor-like score, while the existence of a prominent monocyte-like signal confers resistance of FLT3-ITD-positive AML cases to sorafenib (Figure S3B).

### Drug family responses

The increased sample size of the harmonized dataset yields numerous correlations of drug response with mutational status that achieve statistical significance compared with waves 1 + 2 alone (65 added associations, 27% increase). However, we next wanted to extract additional signal by organizing drug response data into groups of inhibitors based on shared targets or pathways. Accordingly, we aggregated drug-target relationship data from the Cancer Targetome (Blucher et al., 2017, 2019; Choonoo et al., 2019) and other sources (Davis et al., 2011) to yield 25 drug

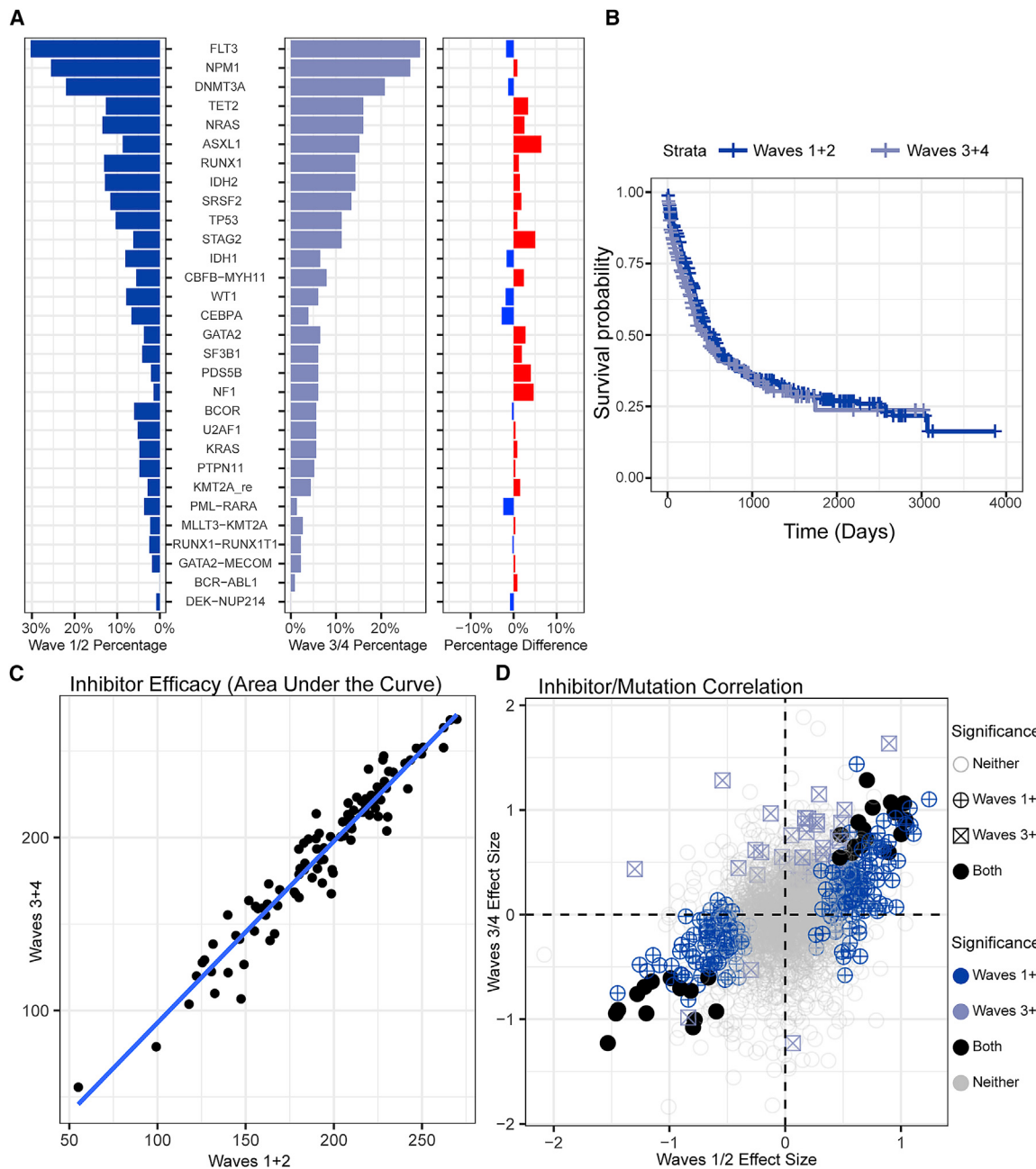


**Figure 1. Genomic features and outcomes for the Beat AML cohorts are concordant**

(A) The percentage of patients with a somatic mutation or gene fusion is shown for waves 1 + 2 and waves 3 + 4 cohorts and percentage difference is shown (average difference is 1.037%).

(B) Overall survival is shown for waves 1 + 2 and waves 3 + 4 cohorts ( $p$  value 0.2, log rank test).

(C) Ex vivo drug response values are shown comparing the average area under the curve (AUC) for each drug (points) within *de novo* AML patients comparing waves 1 + 2 with waves 3 + 4 (Pearson's correlation  $r = 0.965$ ).

(D) Waves 3 + 4 can serve as validation cohort to assess prior mutation-inhibitor associations (Tyner et al., 2018). The difference in average response of specimens that are mutated versus wild type for a given gene (effect size) are plotted for waves 1 + 2 on the x axis and waves 3 + 4 on the y axis. Effect sizes were expressed as Glass's delta with respect to the wild-type group. Significance was based on the Welch's t test comparing mutated versus wild type and requiring a minimum of five mutations in waves 1 + 2 and three mutations in waves 3 + 4. Adjusted significance in waves 1 + 2, waves 3 + 4, or both are also annotated ( $q$  value  $< 0.05$ ; Storey and Tibshirani, 2003).

families with some overlap of drugs between families based on known polypharmacology (Table S4). We observed variable overall response of drug families across all samples tested, with some

families (e.g., phosphatidyl inositol 3' kinase-related kinases [PIKKs]) showing greater overall activity and others (e.g., Aurora kinase [AurK]) showing generally less sensitivity (Figure 4A). By

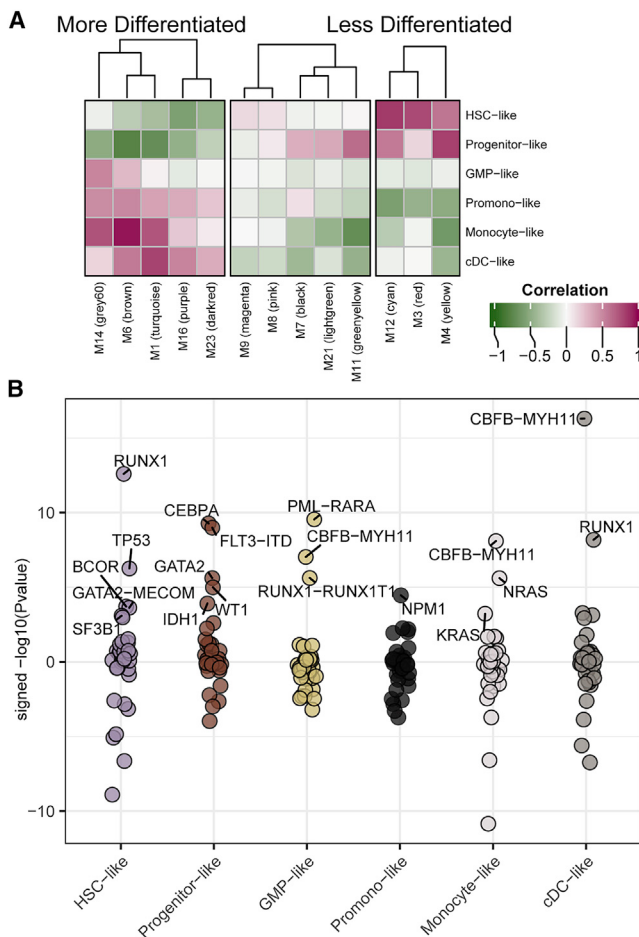


**Figure 2. Differentiation scoring to characterize expression and mutational patterns**

We generated malignant cell-type gene expression scores for each of our patients relative to six sets of 30 genes derived from expression signatures from single-cell sequencing (Van Galen et al., 2019).

(A) By examining the correlation of expression module eigengenes and the cell-type scores we can see that WGCNA expression modules (x axis) show correlation with differentiation cell-type scores (y axis). Pearson's correlation  $r$  values are annotated.

(B) Similarly, we can determine the mutational events significantly associated with each of the cell-type scores. Shown are the signed  $-\log_{10}$  (Welch's t test p values) for the differences in cell-type score with respect to mutational status. Up to the top five most significant ( $q$  value  $<0.05$ ; Storey and Tibshirani, 2003) mutational events associated with enrichment of each cell-type score are highlighted. Full data are available in Table S2.

examining the response of each drug family in specimens with wild-type versus mutated status, we were able to identify numerous instances where mutational events exhibit significantly greater sensitivity or resistance to drug family classes (Figure 4B; for all associations see Table S5). In addition to expected associations such as FLT3-ITD with type III receptor tyrosine kinase (RTK) inhibitors and RAS mutations with STE7 (MEK) inhibitors, we identified numerous unexpected associations, including several treatment-refractory genetic subtypes (mutation of TP53, stromal antigen 2 (STAG2), RUNX1) showing greater sensitivity to phosphatidylinositol kinase family (PIK) inhibitors and

N/KRAS mutation conferring greater sensitivity to cyclin-dependent kinase inhibitors. We also assessed correlations between drug family activity and tumor cell-type scores and found strong correlations with one or more tumor cell-type signatures for 18 out of the 25 drug families (Figure 5A; for all associations see Table S6). Finally, we also observed a number of drug family correlations with cell-type scores that were conditional on mutational/cytogenetic events, such as for PIK family inhibitors showing strong activity against NPM1-mutated cases that also exhibit a high cDC-like score, but PIK inhibitor resistance for NPM1-mutated cases with high HSC-like scores (Figure 5B).

### Determinants of clinical outcome

Finally, we wanted to explore correlations between the WGCNA expression modules and cell-type scores with clinical variables in our dataset, including overall survival, tumor burden and cell composition, age, transformed or therapy-related status, and prognostic categories. To ensure robust associations with overall survival, we limited this analysis to samples collected at initial acute leukemia diagnosis and with RNA-seq data ( $n = 435$ ). Clustering of these features revealed one branch that contained three WGCNA modules (3, 9, and 12) as well the HSC-like cell-type score that associated with shorter overall survival (Figure 6A). Of these, modules 3 and 9 showed the strongest associations with survival. We prioritized the genes in module 3 ( $n = 203$ ) and module 9 ( $n = 119$ ) by computing the correlation with the eigengene (termed kME; Fuller et al., 2007) to quantify each gene's degree of hub status. This revealed a single gene, platelet endothelial aggregation receptor 1 (PEAR1), that correlated far more strongly with the module 3 eigengene than did any other module gene member (Figure 6B). No similar singular driver gene was identified for module 9. Additionally, both module 3 and PEAR1 expression were positively correlated with HSC-like score (Figure 6B; a full list of module component genes is in Table S7). We next applied conditional inference forest methodology (cforest; Hothorn et al., 2006) to understand the relative importance of patient age, WGCNA module eigengenes, cell-type scores, and mutational/cytogenetic status on overall survival. For this analysis, we placed a further restriction to only evaluate cases of *de novo* AML ( $n = 298$ ) because of the observed association between AML type and other variables. Validating known risk factors, this methodology identified age and mutated TP53 (Papaemmanuil et al., 2016) as being among the strongest predictors of survival. However, the WGCNA module 3 was also included as one of the strongest predictors of poor outcome. For young (<45 years) and TP53-wild type middle (45–60 years) age group patients, our analysis revealed module 3 expression to be the strongest determinant of outcome (Figure 6C).

We next explored association of individual PEAR1 gene expression with clinical parameters, since PEAR1 was so strongly associated with the overall module 3 score. Assessment of PEAR1 expression as it relates to European LeukemiaNet (ELN) prognostic categories indicated a significant difference in PEAR1 expression between adverse and favorable risk categories in patients aged 60 years and older (3.765 mean increase in adverse;  $p = 3.276 \times 10^{-25}$ ;  $N = 172$ ). PEAR1 expression, however, shows a smaller but significant difference in the middle age group (1.497 mean increase;  $p = 0.006$ ;  $N = 72$ ) and is not significantly associated with adverse versus favorable ELN risk

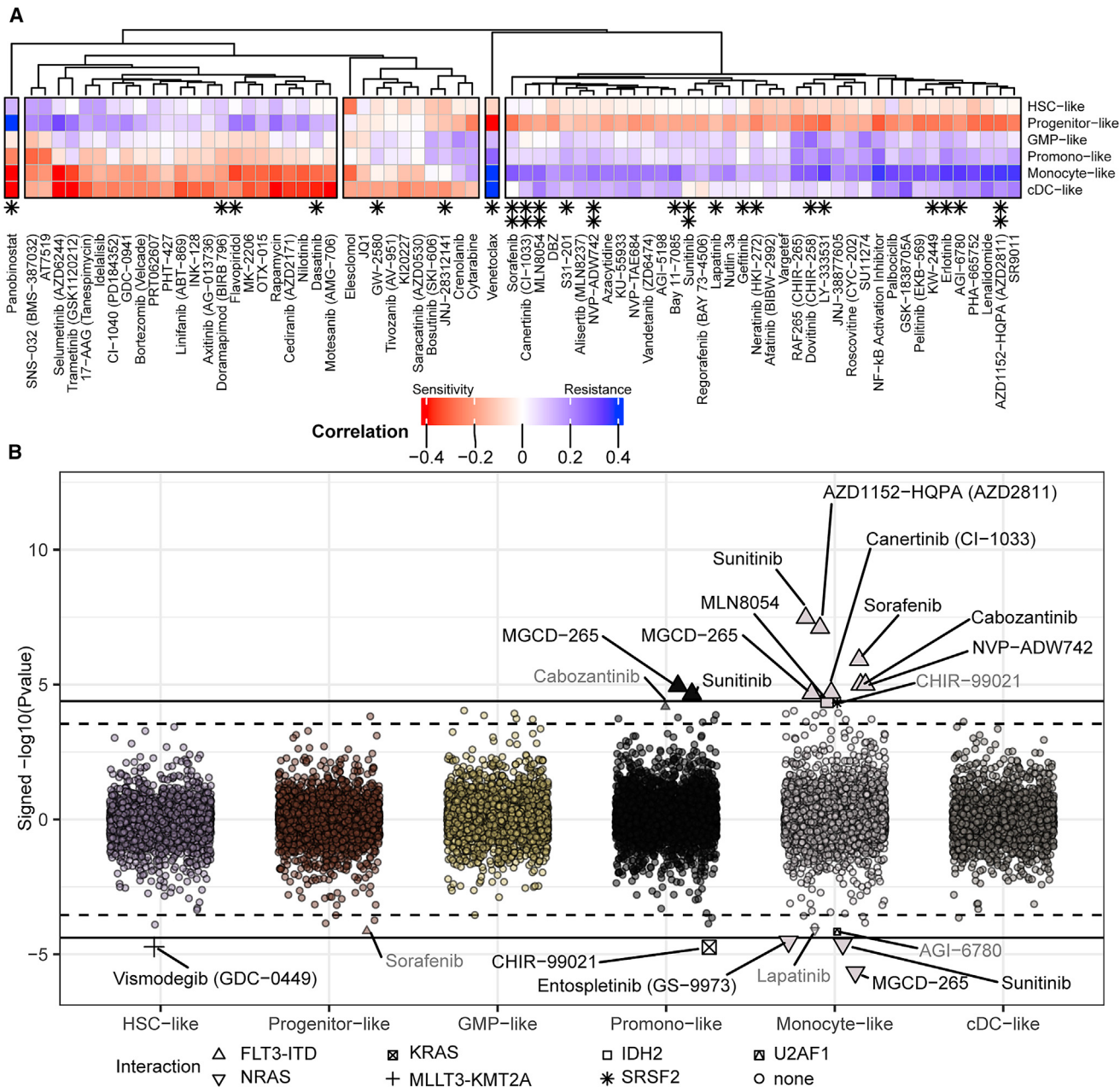


**Figure 3. Influence of cell type on inhibitor response**

(A and B) (A) We compared the cell-type gene expression scores, developed in Figure 2, with ex vivo drug response. Pearson's correlation of ex vivo inhibitor response (measured by AUC) with each of the six cell-type scores reveals relationship between differentiation and resistance (blue) or sensitivity (red). Note, all drugs displayed in the heatmap showed a significant correlation with at least one cell-type (Benjamini and Yekutieli [BY] false discovery rate [FDR]  $<0.05$ ; Benjamini and Yekutieli, 2001). Panobinostat and venetoclax are shown correlated with monocyte-like score in Figure S3A. Asterisks indicate those inhibitors in which there is an interaction between mutation and cell type, shown in (B) (single asterisk,  $q$  value  $<0.1$ ; double asterisk,  $q$  value  $<0.05$ ; Storey and Tibshirani, 2003). Full data are available in Table S3. (B) We examined whether correlations between drug response and cell-type score changed due to mutational status. Drug response modification was quantified by examining the significance (y axis) of the interaction between each mutational event and cell type (x axis) for each inhibitor, requiring a minimum of 10 mutations. Interactions with  $q$  value at two thresholds ( $q < 0.1$ ;  $q < 0.05$ ) are called out by text and shape and distinguished by a dashed and solid line, respectively. As an example, the conditional relationships between sorafenib, FLT3-ITD, and cell-type scores are shown in Figure S3B, where sorafenib activity is robust in FLT3-ITD cases with a high progenitor-like score, but activity is lost in FLT3-ITD cases with a high monocyte-like score.

in young patients ( $p = 0.170$ ;  $N = 79$ ) despite its strong association with outcome in this group (Figure 7A). We compared PEAR1 expression with the leukemic stem cell 17-gene signature

(LSC17) (Ng et al., 2016) in this young subset of patients and found that expression of the single PEAR1 gene could distinguish outcomes in young patients to a similar degree as the 17-gene

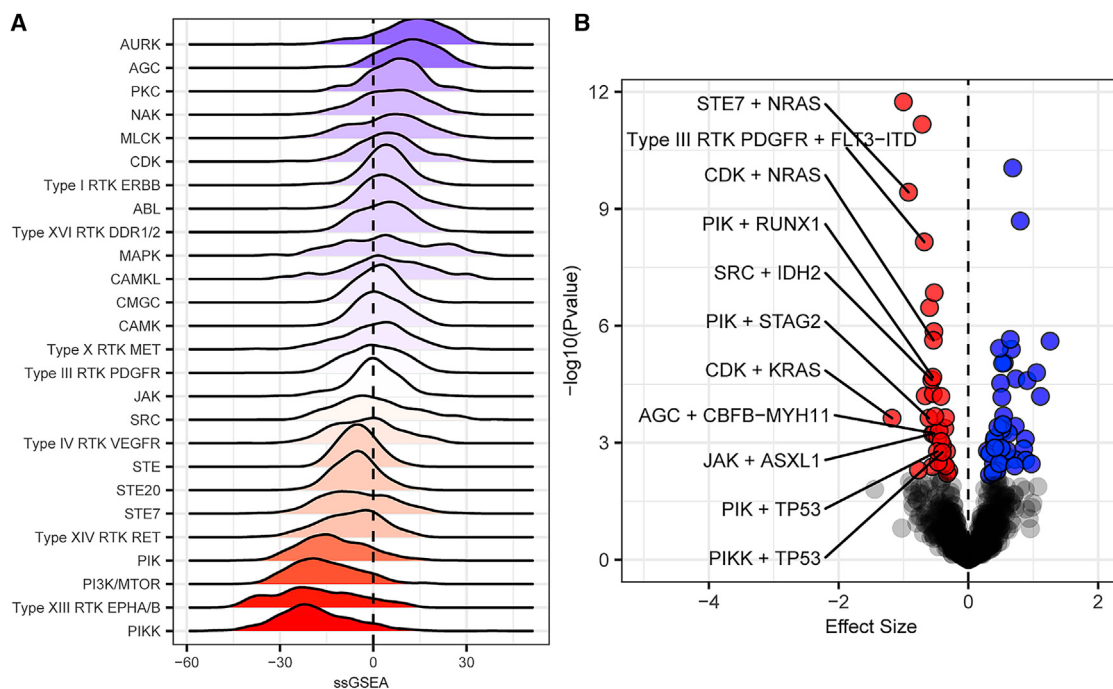


**Figure 4. Genomic associations of drug family response**

As in Figure 3A, we define sensitivity by red and resistant with blue, and with white indicating intermediate.

(A) Drug target information, where available, was annotated for all drugs on the panel, and these targets were mapped onto pathways to create drug families that share common targets and pathways. Full mapping of drug families is available in Table S4. Family-level drug response summaries allow us to identify cohort-level responses. Some, like the Aurora kinase (AurK) family, show overall resistance and others, like type XIII RTKs (Eph) or PIKK, are overall sensitive.

(B) We examined correlations between mutational status and drug family response. Mutational status associates with drug family response either in terms of significant ( $q$  value  $<0.05$ ; [Storey and Tibshirani, 2003](#)) sensitivity (red) or resistance (blue). Association tests were performed using Welch's t test comparing mutated versus wild type and requiring at least five mutations for a given mutational event. Effect size was based on Glass's delta using wild type as the reference. Full data are available in Table S5.

LSC17 signature (Figure 7B). To further compare PEAR1 with LSC17, we assessed the hazard ratio for PEAR1 and LSC17 in all age groups and in the young subset. Additionally, we further stratified cases where the specimen obtained was a bone marrow aspirate, due to improved splitting of outcomes observed with bone marrow compared with peripheral blood specimens (Figure S4). The hazard ratios reveal similar performance of PEAR1 with LSC17 (Figure 7C), noting predictive range is influenced by subset and split type. Since PEAR1 shows strong upregulation in transformed AML, which is known to exhibit inferior outcome (Figures 6A, S5A, and S5B), and since a similar association was observed with LSC17 and transformed AML ( $p = 2.18 \times 10^{-7}$ ), we wanted to compare PEAR1 and LSC17 in all cases with specimens obtained at initial acute leukemia diagnosis, inclusive of transformed and therapy-related AML cases. This analysis revealed PEAR1 to perform equivalently to LSC17 both in the young subset and across all age groups (Figure S6). Finally, to validate the prognostic significance of PEAR1 using independent patient cohorts, we examined the capacity of PEAR1 expression to stratify overall survival using a dataset from Malani and coworkers as well as from The Cancer Genome Atlas (TCGA) (Cancer Genome Atlas Research et al., 2013; Malani et al., 2022). We found that elevated PEAR1 expression conferred shortened overall survival in a strongly significant manner in both datasets (Figures S7A and S7B).

## DISCUSSION

The impact of AML LSCs on tumor biology and therapeutics has been explored and suggested to prime disease pathogenesis and seed relapse. However, a broader and more nuanced understanding of the full range of AML tumor cell maturation states, and the way in which these different cell states are tied to other disease features such as genetics and drug response, has been lacking. While some of these maturation states were roughly captured in the historical FAB classification system for AML, this system has been all but abandoned in current classification schemes that utilize primarily (or only) genetics and prior clinical history (Arber et al., 2016; Dohner et al., 2017). In addition, while targeting of LSCs has been a major goal for AML research with the notion that eliminating LSCs would induce tumor collapse, this result has proved elusive with the observation that relapse can be seeded by more mature cells, depending on the administered therapy. Through broad mapping of distinct AML cell maturation states with both genetic features and response to broad families of drugs, we find that tumors can display features of multiple, disparate cell maturation states and that a majority of drugs and drug families exhibit cell maturation state-biased response. Our expansive modeling of clinical outcome has also led to a single, targetable gene that is a strong determinant of overall survival in AML, PEAR1.

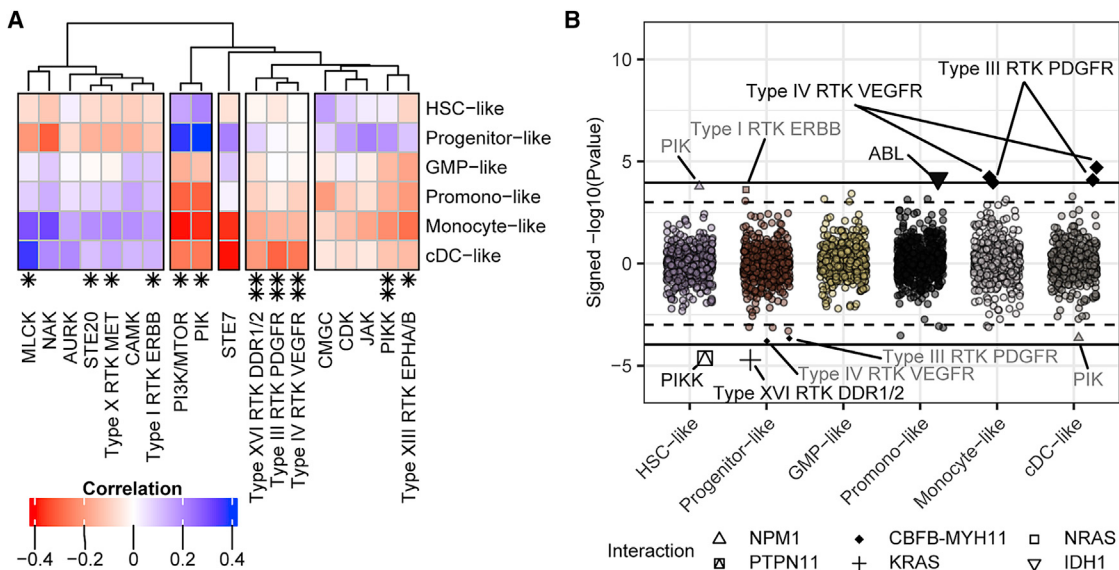


**Figure 5. Drug family response is influenced by and conditional on cell type**

(A) Similar to the analysis of single-inhibitor responses and their correlation with cell-type score, shown in Figure 3A, we can group the drug families from Figure 4 by their association with cell-type differentiation scores based on their Pearson's correlation (BY FDR <0.05; Benjamini and Yekutieli, 2001).

(B) We can also determine instances where drug family correlation with mutational state is conditional on cell type (as we did for individual drugs in Figure 3B). The mutations that play a significant drug response modification role based on the statistical interaction between cell-type score and mutation, requiring at least 10 mutations per event, is shown. The y axis indicates the signed  $-\log_{10}(p\text{ value})$ , and the x axis indicates cell type. The interactions are listed by text (q value <0.1 and q value <0.05; Storey and Tibshirani, 2003) and distinguished by a dashed and solid line respectively. Full data are available in Table S6.

PEAR1, also known as JEDI or MEGF12, was originally identified to signal during platelet aggregation (Nanda et al., 2005) and is a homolog of Draper (*Drosophila melanogaster*) and ced-1 (*Caenorhabditis elegans*). It is a type I transmembrane protein with 15 extracellular epidermal growth factor-like repeats, a domain sharing homology with NOTCH ligands, and it contains tyrosine and serine residues that can become phosphorylated (Krivtsov et al., 2007; Nanda et al., 2005). Genetic polymorphisms in the PEAR1 locus associate with cardiovascular events, response to anti-platelet aggregation therapies (Eicher et al., 2016; Faraday et al., 2011; Herrera-Galeano et al., 2008; Johnson et al., 2010; Jones et al., 2009; Lewis et al., 2013), and endothelial cell biology (Fisch et al., 2015; Vandenbriele et al., 2015; Zhan et al., 2020). Methylation of the PEAR1 locus correlates with megakaryopoiesis and platelet function (Izzi et al., 2016, 2018, 2019). On glial precursor cells, PEAR1 triggers clathrin-dependent engulfment of apoptotic neurons generated during development of peripheral ganglia (Sullivan et al., 2014; Wu et al., 2009). This phagocytic process signaling involves spleen associated tyrosine kinase (SYK), SRC proto-oncogene, non-receptor tyrosine kinase (SRC)-family kinases, and MAPK8 (JNK; JUN N-terminal kinase) and/or their *D. melanogaster* homologs (Hilu-Dadia et al., 2018; Scheib et al., 2012). PEAR1 ligands include Fc epsilon receptor Ia (Sun et al., 2015), dextran sulfate (Vandenbriele et al., 2016), and sulfated fucose-based polysaccharides (fucoidans) (Kardebey et al., 2019), and signaling in platelets involves SRC-family kinases and PI3C/AKT (Kauskot et al., 2012, 2013). In healthy hematopoietic cells, PEAR1 expression is highest in HSCs and in megakaryocyte-erythroid progenitor cells. Forced expression of PEAR1 in bone marrow cells or in fibroblast stromal cells was

shown to reduce clonogenic myeloid colony formation (Krivtsov et al., 2007). This effect seems counterintuitive given the clear association of elevated PEAR1 expression with worse outcome in AML and warrants further investigation.

A recent study examined AML TCGA (Cancer Genome Atlas Research et al., 2013) to identify an immune prognostic signature for AML, which included PEAR1 as well as another gene, PYD and CARD domain containing (PYCARD) (Dao et al., 2021). This model showed correlation with T cell enrichment and expression of immune checkpoints. It was also shown to correlate with poor clinical outcome in several AML datasets; however, a role for PEAR1 in shaping leukemic cell biology or cell type was not considered.

Here, we show that PEAR1 expression predicts outcome in young AML patients independently of ELN category, performs equivalently to the LSC17 gene signature, and correlates strongly with an HSC-like signature. Increased PEAR1 was confirmed in cases with mutation of TP53, RUNX1, and ASXL transcriptional regulator 1 (ASXL1) (as shown in Dao et al., 2021), and we also observe elevation in other genetic subsets with poor prognostic markers (serine and arginine rich splicing factor 2 [SRSF2] mutation, GATA binding protein 2-MDS1 and EVI1 complex locus [GATA2-MECOM]) and lower expression with certain good prognostic features (NPM1, CCAAT enhancer binding protein alpha [CEBPA]) (Figure S5C). Finally, while there was an increasing trend in expression of initial diagnosis PEAR1 across ethnicities (non-Hispanic white, mean 1.395, N = 359; African heritage, mean 2.205, N = 13), the smaller sample size in the non-Caucasian groups warrants further investigation in a validation cohort. This is potentially important

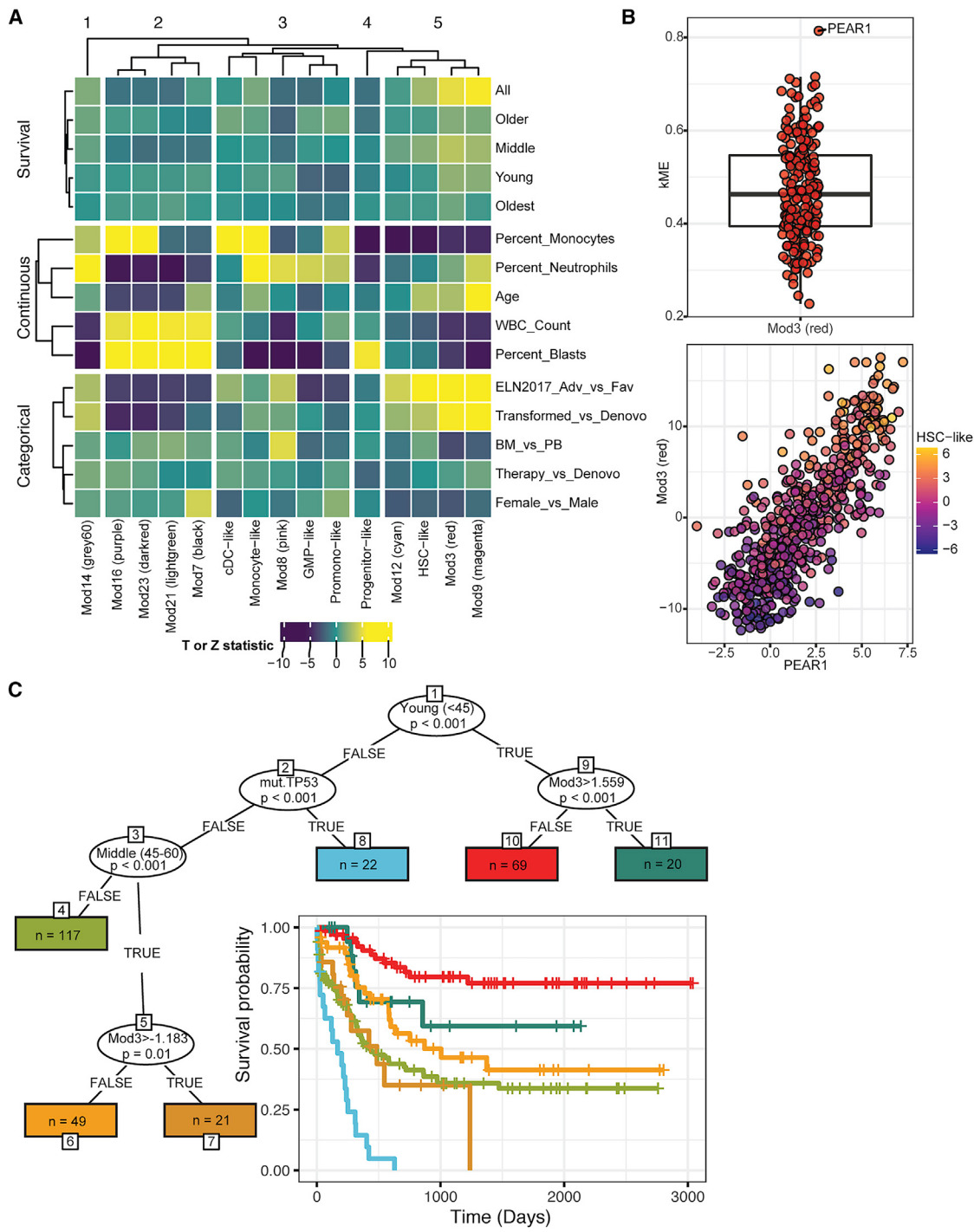


**Figure 6. Comprehensive analysis of clinical variables identifies PEAR1 expression as a prognostic factor in AML**

(A) We analyzed univariate associations between the six cell-type scores and the set of nine non-redundant WGCNA eigengenes with categorical and continuous clinical variables as well as overall survival across and within age subsets. Each variable type was grouped on the y axis and the displayed association values were derived from the corresponding test statistics. These include the Z statistic for categorical (logistic regression) and survival outcomes (Cox proportional hazards) and T statistic for the continuous outcomes (general linear model). Average linkage hierarchical clustering was applied to rows (within groups) and columns.

(B) (Top) To understand which gene(s) among the module 3 WGCNA signature are the strongest drivers of the overall signature, we calculated the correlation of each gene with the module eigengene (kME). Of all the 203 genes in module 3, PEAR1 has the highest correlation. (Bottom) The patient expression values (dots) of PEAR1 (x axis) correlated highly with the Mod3 module eigengene (y axis) and both are also correlated with the HSC-like malignant cell type as indicated by the cell-type purple (low) to yellow (high) gradient as defined in Figure S2A. Full module gene components are available in Table S7.

(legend continued on next page)

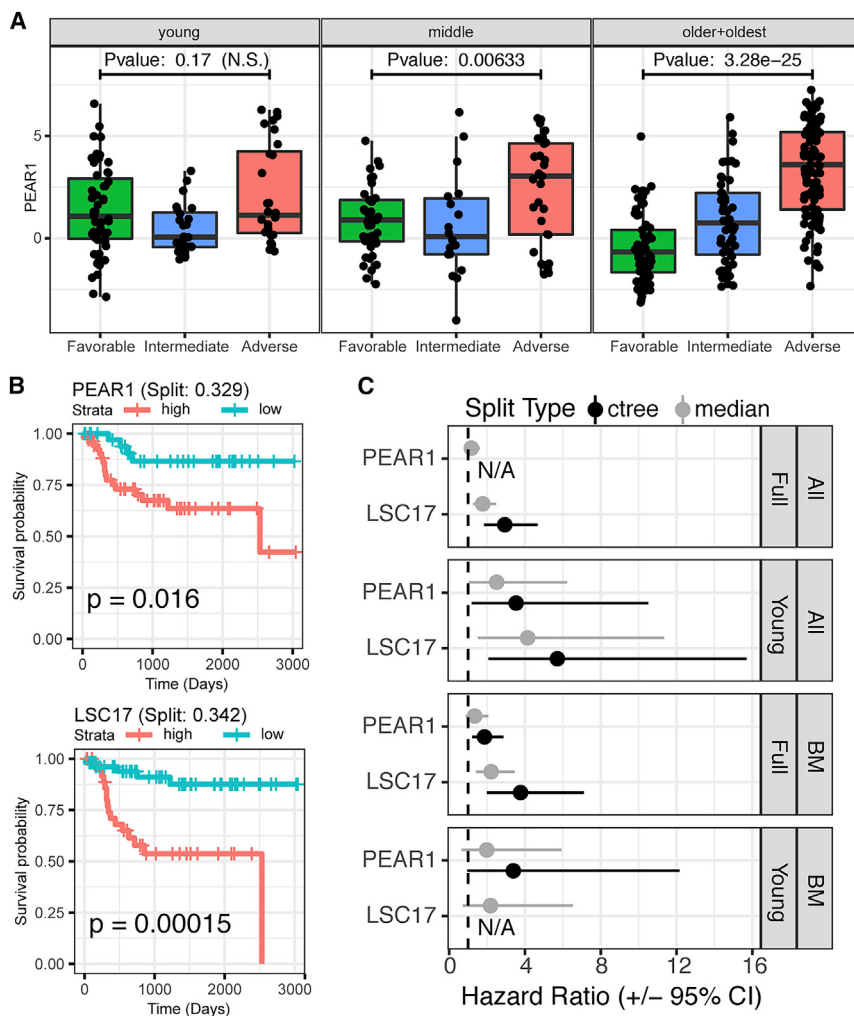


**Figure 7. Integrative modeling shows PEAR1 expression is a single, independent predictor of poor prognosis**

(A) PEAR1 expression (y axis) is significantly higher in adverse compared with favorable ELN 2017 risk categorization (x axis) for patients aged 60 years and over (dots; older + oldest group), but the pattern is less pronounced in patients aged <60 years. Significance determined using a Welch's t test.

(B) PEAR1 expression differentiates survival for young patients equivalently to the LSC17 signature. Categorization of samples into high and low expression groups for PEAR1 and LSC17 was determined using the ctree methodology to facilitate comparison with PEAR1.

(C) We compared performance of PEAR1 and LSC17 using both ctree and the median expression values for each. Shown are the hazard ratios (HRs) and 95% confidence intervals (CIs) for PEAR1 and LSC17 in the entire cohort or in the younger patients as well as in all sample types or only in bone marrow samples. The categories were high versus low expression as determined by either median threshold or significant splits using ctree (i.e., split type). In two instances, the ctree method failed to identify a split, and these are denoted with N/A.

due to recent findings of outcome disparities among black AML patients (Bhatnagar et al., 2021) as well as several studies reporting racially skewed representation of PEAR1 polymorphisms that affect PEAR1 expression/function (Herrera-Galeano et al., 2008; Keramati et al., 2019; Qayyum et al., 2015).

Elevation of PEAR1 expression in ASXL1-mutated AML is notable, since ASXL1 is commonly mutated in clonal hematopoiesis, which is also associated with elevated cardiovascular events (Genovese et al., 2014; Jaiswal et al., 2014). As noted above, PEAR1 genetics and function have been tied to the biology of cardiovascular events, raising the intriguing possibility that these findings could be connected. Platelet levels have been shown to decline with age (Biino et al., 2013), and a leukocyte pool with enhanced platelet aggregation potential—possibly facilitated by increased PEAR1 downstream of somatic muta-

tional events such as ASXL1—could represent a selective advantage within an aging hematopoietic microenvironment. All of these data raise the possibility of PEAR1 as a therapeutic target. Since PEAR1 may function as an active signaling protein, small molecules could mitigate PEAR1 signaling. Antibodies to PEAR1 have been developed, so a large-molecule approach may also be feasible. Indeed, we have performed preliminary validation of this concept by showing PEAR1 surface expression on tumor cells from AML patient samples (Figure S7C) with the degree of surface expression strongly correlated with PEAR1 transcript levels (Figure S7D). Interruption of normal PEAR1 function must be considered for any targeting strategy; however, platelet function was not compromised in a PEAR1-null mouse (Crikel et al., 2016).

There are other important limitations to consider. First, the prognostic significance of PEAR1 has, thus far, been demonstrated in datasets where therapies employed were almost entirely anthracycline based. As drug regimens are now more diversified, it will be important to study the prognostic significance of PEAR1 in patients receiving alternative treatments. In this sense, and in general, the clinical utility of measuring

(C) A strategy based on a forest of conditional inference trees (cforest) was used to determine variables that differentiate overall survival. Age groups, expression modules (denoted with Mod\*), gene mutation, AML gene fusions, and cell-type scores from the harmonized dataset were all included in the model. The age groups are young (<45 years), middle (45–60 years), older (60–75 years), and oldest (>75 years). Depiction of the resulting tree where oval splits indicate variables that most significantly split overall survival. Lines indicate values that were split on, for instance, “TRUE” for the “young” variable, which indicates that the subgroup is <45 years old. The resulting subgroups of patients, rectangles that denote terminal nodes, are listed with the subgroup size (denoted as n) and are colored to match corresponding survival curves.

PEAR1 expression for prognostication and/or of therapeutically targeting PEAR1 must be confirmed in future clinical studies.

Collectively, this study exemplifies the utility of integrative analysis that incorporates functional testing of large cohorts of patient specimens. This includes broad association of drug sensitivity with tumor cell differentiation state and drug/mutation correlations that are sometimes conditional on cell type. Given the strong associations that can be seen between cell-type score and drug response, the distribution of these cell phenotypes should be assessed when evaluating clinical differences in drug sensitivity. Testing interactions between cell type and other disease or patient features can help identify potential confounders or modifiers of drug response. For key comparisons, cell-type consideration should be done as routinely as population substructure adjustment. Finally, our analysis of clinical outcome has yielded a prognostic and potentially targetable feature of AML that merits further testing and exploration.

## STAR★METHODS

Detailed methods are provided in the online version of this paper and include the following:

- [KEY RESOURCES TABLE](#)
- [RESOURCE AVAILABILITY](#)
  - Lead contact
  - Materials availability
  - Data and code availability
- [EXPERIMENTAL MODEL AND SUBJECT DETAILS](#)
  - Patient sample collection and cohort organization
- [METHOD DETAILS](#)
  - Patient specimen processing
  - DNA sequencing
  - European leukemia network prognostic categorization
  - *Ex vivo* functional drug Screen data processing
  - Organization of drugs into families based on targets and pathways
  - Inhibitor family response
  - RNA sequencing
  - Weighted gene Co-expression network analysis
  - Cell-type scores
  - Formation of genomic features
  - Random survival forest
  - LSC17
  - Clinical curation via natural language processing (NLP)
  - PEAR1 flow cytometry analysis
- [QUANTIFICATION AND STATISTICAL ANALYSIS](#)
- [ADDITIONAL RESOURCES](#)

## SUPPLEMENTAL INFORMATION

Supplemental information can be found online at <https://doi.org/10.1016/j.ccr.2022.07.002>.

## ACKNOWLEDGMENTS

We thank all of our patients at all sites for donating precious time and tissue. DNA and RNA quality assessments, library creation, and short-read sequencing assays were performed by the OHSU Massively Parallel

Sequencing Shared Resource. We thank Oscar Brück, Disha Malani, Olli Kalioniemi, and Kimmo Porkka for rapidly facilitating analysis of PEAR1 expression correlation with overall survival in their AML patient dataset ([Malani et al., 2022](#)) and Oscar Brück for rapidly executing our analysis scripts from this study on those data. Funding for this project was provided in part by The Leukemia & Lymphoma Society (for the waves 1 + 2 dataset) and the Knight Cancer Research Institute (OHSU). Supported included grants from the National Cancer Institute (U01CA217862, U54CA224019, U01CA214116) and NIH/NCATS CTSA UL1TR002369 (S.K.M., B.W.). C.E.T. receives grant support from the National Cancer Institute (R01CA214428). A.A. is supported by grants from the National Cancer Institute (R01CA229875), National Heart, Lung, and Blood Institute (R01HL155426), American Cancer Society (RSG-17-187-01-LIB), Alex Lemonade/Babich RUNX1 Foundation, EvansMDS Foundation, and a V foundation Scholar award. Funding was provided to T.P.B. by an American Society of Hematology Research Restart Award, an American Society of Hematology Scholar Award, and one K08 CA245224 from NCI. S.K.J. is supported by the ARCS Scholar Foundation, The Paul & Daisy Soros Fellowship, and the National Cancer Institute (F30CA239335). J.E.M. receives funding from the American Cancer Society (RSG-19-184-01 – LIB) and NIH/NCI (R01 CA247943). H.Z. received grants from the National Cancer Institute (R00 5K99CA237630) and the Oregon Medical Research Foundation New Investigator Award. Some patient samples used in this work were provided by the Division of Hematology Biorepository at Huntsman Cancer Institute, University of Utah, which is supported by the National Cancer Institute of the National Institutes of Health under award number P30CA042014. Additional funding came from the Huntsman Center of Excellence in Hematologic Malignancies and Hematology at Huntsman Cancer Institute, University of Utah. C.R.C. received a Scholar in Clinical Research Award from The Leukemia & Lymphoma Society (2400-13), and was distinguished with a Pierre Chagnon Professorship in Stem Cell Biology and Blood & Marrow Transplant and a UF Research Foundation Professorship. This work was supported in part by the Intramural Research Program of the National Heart, Lung, and Blood Institute of the National Institutes of Health. B.J.D. received funding from the Howard Hughes Medical Institute. J.W.T. received grants from the V Foundation for Cancer Research, the Gabrielle's Angel Foundation for Cancer Research, the Mark Foundation For Cancer Research, the Silver Family Foundation, and the National Cancer Institute (R01CA245002, R01CA262758).

## AUTHOR CONTRIBUTIONS

D.B., N.L., A.R.S., S.E.K., C.E.T., K.J., B.J.D., S.K.M., and J.W.T. provided project oversight for experimental design, data management, integration, and data analysis and interpretation. D.B. co-led the modeling, analysis, and data visualizations; developed computational workflows for pre-processing, harmonization, and analysis of RNA-seq and Exome-seq; co-developed the workflow and extensions for *ex vivo* drug screening; assisted with clinical data curation; serves as co-developer and current maintainer of the Vizome platform; and led the dissemination efforts. N.L. led the management, curation, entry, quality assurance and quality control, validation, and analysis of patient clinical annotations. A.R.S. led patient sample processing; assisted with *ex vivo* drug screening, DNA/RNA extractions, and sequencing sample submissions; and managed sequencing mismatch findings. S.E.K. provided oversight for and assisted with collection of *ex vivo* drug response data and analysis and led the development of methodology for and collection of FLT3 and NPM1 in/del data. K.J. provided project oversight and management, and assisted with patient sample processing and *ex vivo* drug screening. C.E.T. and J.W.T. conceived the project and provided project oversight for sample accrual and collection as well as experimental methods development. B.J.D. conceived the project and provided project oversight. S.K.M. co-led the modeling, analysis, and visualizations, and provided oversight for computational methods development and the development of the Vizome platform as well as oversight for data governance and dissemination.

T.P.B., U.B., B.H.C., R.C., A.D., K.-H.T.D., M.M.L., J.N.S., E.T., J.T., A.D.P., and S.E.S. assisted with patient sample acquisition. T.P.B. and A.D.P. assisted with patient sample coordination. E.T. assisted with clinical data structure,

collection, and analysis. M.M.L. assisted with IRB protocol development and maintenance, clinical data structure, collection, and analysis. A.d'A., M.A., S.A., J.B., J. Bryant, R.B., C.C., H.J.C., S.C., M.D., I.E., H. Ho, S.K.J., Y.K., H.L., S.L., S. Luty, A.M., J.M., Q.M., A.R., A. Rogers, D.A.S., R.L.S., T.S., A.T., K.T.-K., J.W., and J. Wolf assisted with patient sample processing and *ex vivo* drug screening. M.A., I.E., and A.R. assisted with DNA/RNA extractions and sequencing sample submissions. B.J. and T.M. provided regulatory oversight. B.J. assisted with curation and entry of patient clinical annotations. P.L. assisted with technology transfer, project development, alliance management, and data management. A.K. and M.M. developed the original *ex vivo* drug screening workflow and A.K. co-developed the extensions of that workflow. J. Minnier contributed to extensions for the *ex vivo* drug screening workflow. D.N. assisted in the creation of the drug screening replicate plates. P.R. assisted with the *ex vivo* drug screening analysis. K.A.R. collected and analyzed PEAR1 flow cytometry data and helped design the graphical abstract.

A.A., B.H.C., C.A.E., E.L., J.M., J.N.S., and H.Z. assisted with data analysis and interpretation. A.B. led the Targetome extensions. T.L. and G.W. assisted with data integration. B.W. assisted with project oversight and conceived the original Vizome platform. C.L., E.C., R.H., and R. Seales assisted with exome and RNA-seq library creation, sequencing, and data processing. A.M.C. and S.H. assisted with clinical curation and natural language processing. J.D. assisted with curation and entry of patient clinical annotations. E.B., H.H., J.R., M.L., R. Schuff, and A.Y. assisted with clinical data integration from the OHSU Research Data Warehouse. A.Y. integrated the *ex vivo* workflow in the Beat AML database.

C.R.C. served as a co-investigator on the repository protocol, obtained consent and collected samples from patients, processed and shipped specimens, aided with clinical annotation, and edited and provided feedback on the manuscript. R.H.C., M.W.D., C.S.H., and T.L.L. served as local principal investigators for the repository protocols, consented patients and collected samples, aided with clinical annotation, and edited and provided feedback on the manuscript. R.T.S. served as a co-investigator on the repository protocol, assisted with data interpretation, and edited and provided feedback on the manuscript. C.T.J. and D.A.P. collected samples for the repository protocol and provided feedback on the manuscript. M.E.M. and R.R.P. consented patients and collected samples for the repository protocol and aided with clinical annotation. J.M.W. served as a local principal investigator for the repository protocol and edited and provided feedback on the manuscript. S.J.W. enabled, facilitated, and mentored basic, translational and clinical research activities arising from data generated by Beat AML at the University of Kansas Cancer Center site and participated in the Beat AML Symposia to share research and create research projects.

### DECLARATION OF INTERESTS

C.E.T. receives research support from Notable Labs and serves as a scientific liaison for AstraZeneca. J.E.M. receives research funding from Gilead Pharmaceutical and serves on a scientific advisory board for Ionis Pharmaceuticals. M.W.D. serves on the advisory boards and/or as a consultant for Novartis, Incyte, and BMS and receives research funding from BMS and Gilead. C.S.H. receives research funding from Sellas. T.L.L. consults for Jazz Pharmaceuticals and receives research funding from Tolero, Gilead, Prescient, Ono, Bio-Path, Mateon, Genentech/Roche, Trovagene, AbbVie, Pfizer, Celgene, Imago, Astellas, Karyopharm, Seattle Genetics, and Incyte. D.A.P. receives research funding from Pfizer and Agios and served on advisory boards for Pfizer, Cel-lyad, Agios, Celgene, AbbVie, Argennx, Takeda, and Servier. B.J.D. serves on the advisory boards for Aileron Therapeutics, Aptose, Blueprint Medicines, Cepheid, EnLiven Therapeutics, Gilead, GRAIL, Iteron Therapeutics, Nemucore Medical Innovations, the Novartis CML Molecular Monitoring Steering Committee, Recludix Pharma, the RUNX1 Research Program, ALLCRON Pharma, VB Therapeutics, Vincerx Pharma, and the Board of Directors for Amgen, and receives research funding from EnLiven and Recludix. B.J.D. is principal investigator or co-investigator on Novartis, BMS, and Pfizer clinical trials. His institution, OHSU, has contracts with these companies to pay for patient costs, nurse and data manager salaries, and institutional overhead, but he does not derive salary, nor does his laboratory receive funds, from these contracts. J.W.T. has received research support from Acerta, Agios, Aptose, Array, AstraZeneca, Constellation, Genentech, Gilead, Incyte, Janssen, Kro-

nos, Meryx, Petra, Schrodinger, Seattle Genetics, Syros, Takeda, and Tolero and serves on the advisory board for Recludix Pharma. The authors certify that all compounds tested in this study were chosen without input from any of our industry partners. A subset of findings from this manuscript have been included in a pending patent application.

Received: February 1, 2022

Revised: May 30, 2022

Accepted: June 30, 2022

Published: July 21, 2022

### REFERENCES

- Arber, D.A., Orazi, A., Hasserjian, R., Thiele, J., Borowitz, M.J., Le Beau, M.M., Bloomfield, C.D., Cazzola, M., and Vardiman, J.W. (2016). The 2016 revision to the World Health Organization classification of myeloid neoplasms and acute leukemia. *Blood* 127, 2391–2405.
- Armstrong, J.F., Faccenda, E., Harding, S.D., Pawson, A.J., Southan, C., Sharman, J.L., Campo, B., Cavanagh, D.R., Alexander, S.P.H., Davenport, A.P., et al. (2020). The IUPHAR/BPS Guide to PHARMACOLOGY in 2020: extending immunopharmacology content and introducing the IUPHAR/MMV Guide to MALARIA PHARMACOLOGY. *Nucleic Acids Res.* 48, D1006–D1021.
- Avila Cobos, F., Vandesompele, J., Mestdagh, P., and De Preter, K. (2018). Computational deconvolution of transcriptomics data from mixed cell populations. *Bioinformatics* 34, 1969–1979.
- Barbie, D.A., Tamayo, P., Boehm, J.S., Kim, S.Y., Moody, S.E., Dunn, I.F., Schinzel, A.C., Sandy, P., Meylan, E., Scholl, C., et al. (2009). Systematic RNA interference reveals that oncogenic KRAS-driven cancers require TBK1. *Nature* 462, 108–112.
- Benjamini, Y., and Yekutieli, D. (2001). The control of the false discovery rate in multiple testing under dependency. *Ann. Statist.* 29, 1165–1188.
- Bennett, J.M., Catovsky, D., Daniel, M.T., Flandrin, G., Galton, D.A., Gralnick, H.R., and Sultan, C. (1976). Proposals for the classification of the acute leukemias. French-American-British (FAB) co-operative group. *Br. J. Haematol.* 33, 451–458.
- Bhatnagar, B., Kohlschmidt, J., Mrózek, K., Zhao, Q., Fisher, J.L., Nicolet, D., Walker, C.J., Mims, A.S., Oakes, C., Giacopelli, B., et al. (2021). Poor survival and differential impact of genetic features of Black patients with acute myeloid leukemia. *Cancer Discov.* 11, 626–637.
- Biino, G., Santimone, I., Minelli, C., Sorice, R., Frongia, B., Traglia, M., Ulivi, S., Di Castelnuovo, A., Gögele, M., Nutile, T., et al. (2013). Age- and sex-related variations in platelet count in Italy: a proposal of reference ranges based on 40987 subjects' data. *PLoS One* 8, e64289.
- Blucher, A.S., Choonoo, G., Kulesz-Martin, M., Wu, G., and McWeney, S.K. (2017). Evidence-based precision oncology with the cancer targetome. *Trends Pharmacol. Sci.* 38, 1085–1099.
- Blucher, A.S., McWeney, S.K., Stein, L., and Wu, G. (2019). Visualization of drug target interactions in the contexts of pathways and networks with ReactomeFIViz. *F1000Res.* 8, 908.
- Cancer Genome Atlas Research Network, Ley, T.J., Miller, C., Ding, L., Raphael, B.J., Mungall, A.J., Fulton, R., Hoadley, K., Triche, T.J., Jr., Laird, P.W., et al. (2013). Genomic and epigenomic landscapes of adult de novo acute myeloid leukemia. *N. Engl. J. Med.* 368, 2059–2074.
- Choonoo, G., Blucher, A.S., Higgins, S., Boardman, M., Jeng, S., Zheng, C., Jacobs, J., Anderson, A., Chamberlin, S., Evans, N., et al. (2019). Illuminating biological pathways for drug targeting in head and neck squamous cell carcinoma. *PLoS One* 14, e0223639.
- Criel, M., Izzi, B., Vandebriele, C., Liesenborghs, L., Van Kerckhoven, S., Lox, M., Cludts, K., Jones, E.A.V., Vanassche, T., Verhamme, P., and Hoylaerts, M. (2016). Absence of PEAR1 does not affect murine platelet function in vivo. *Thromb. Res.* 146, 76–83.
- Dao, F.T., Wang, J., Yang, L., and Qin, Y.Z. (2021). Development of a poor-prognostic-mutations derived immune prognostic model for acute myeloid leukemia. *Sci. Rep.* 11, 4856.

- Davis, M.I., Hunt, J.P., Herrgard, S., Ciceri, P., Wodicka, L.M., Pallares, G., Hocker, M., Treiber, D.K., and Zarrinkar, P.P. (2011). Comprehensive analysis of kinase inhibitor selectivity. *Nat. Biotechnol.* 29, 1046–1051.
- DiNardo, C.D., Pratz, K., Pullarkat, V., Jonas, B.A., Arellano, M., Becker, P.S., Frankfurt, O., Konopleva, M., Wei, A.H., Kantarjian, H.M., et al. (2019). Venetoclax combined with decitabine or azacitidine in treatment-naïve, elderly patients with acute myeloid leukemia. *Blood* 133, 7–17.
- DiNardo, C.D., Stein, E.M., de Botton, S., Roboz, G.J., Altman, J.K., Mims, A.S., Swords, R., Collins, R.H., Mannis, G.N., Pollyea, D.A., et al. (2018). Durable remissions with ivosidenib in IDH1-mutated relapsed or refractory AML. *N. Engl. J. Med.* 378, 2386–2398.
- Döhner, H., Estey, E., Grimwade, D., Amadori, S., Appelbaum, F.R., Büchner, T., Dombret, H., Ebert, B.L., Fenaux, P., Larson, R.A., et al. (2017). Diagnosis and management of AML in adults: 2017 ELN recommendations from an international expert panel. *Blood* 129, 424–447.
- Eicher, J.D., Chami, N., Kacprowski, T., Nomura, A., Chen, M.H., Yanek, L.R., Tajuddin, S.M., Schick, U.M., Slater, A.J., Pankratz, N., et al. (2016). Platelet-related variants identified by exomechip meta-analysis in 157,293 individuals. *Am. J. Hum. Genet.* 99, 40–55.
- Elsayed, A.H., Rafiee, R., Cao, X., Raimondi, S., Downing, J.R., Ribeiro, R., Fan, Y., Gruber, T.A., Baker, S., Klico, J., et al. (2020). A six-gene leukemic stem cell score identifies high risk pediatric acute myeloid leukemia. *Leukemia* 34, 735–745.
- Falini, B., Nicoletti, I., Martelli, M.F., and Mecucci, C. (2007). Acute myeloid leukemia carrying cytoplasmic/mutated nucleophosmin (NPMc+ AML): biologic and clinical features. *Blood* 109, 874–885.
- Faraday, N., Yanek, L.R., Yang, X.P., Mathias, R., Herrera-Galeano, J.E., Suktutipat, B., Qayyum, R., Johnson, A.D., Chen, M.H., Tofler, G.H., et al. (2011). Identification of a specific intronic PEAR1 gene variant associated with greater platelet aggregability and protein expression. *Blood* 118, 3367–3375.
- Fisch, A.S., Yerges-Armstrong, L.M., Backman, J.D., Wang, H., Donnelly, P., Ryan, K.A., Parikh, A., Pavlovich, M.A., Mitchell, B.D., O'Connell, J.R., et al. (2015). Genetic variation in the platelet endothelial aggregation receptor 1 gene results in endothelial dysfunction. *PLoS One* 10, e0138795.
- Fuller, T.F., Ghazalpour, A., Aten, J.E., Drake, T.A., Lusis, A.J., and Horvath, S. (2007). Weighted gene coexpression network analysis strategies applied to mouse weight. *Mamm. Genome* 18, 463–472.
- Gal, H., Amariglio, N., Trakhtenbrot, L., Jacob-Hirsh, J., Margalit, O., Avigdor, A., Nagler, A., Tavor, S., Ein-Dor, L., Lapidot, T., et al. (2006). Gene expression profiles of AML derived stem cells; similarity to hematopoietic stem cells. *Leukemia* 20, 2147–2154.
- Genovese, G., Kähler, A.K., Handsaker, R.E., Lindberg, J., Rose, S.A., Bakhour, S.F., Chambert, K., Mick, E., Neale, B.M., Fromer, M., et al. (2014). Clonal hematopoiesis and blood-cancer risk inferred from blood DNA sequence. *N. Engl. J. Med.* 371, 2477–2487.
- Gentles, A.J., Plevritis, S.K., Majeti, R., and Alizadeh, A.A. (2010). Association of a leukemic stem cell gene expression signature with clinical outcomes in acute myeloid leukemia. *JAMA* 304, 2706–2715.
- Hansen, K.D., Irizarry, R.A., and Wu, Z. (2012). Removing technical variability in RNA-seq data using conditional quantile normalization. *Biostatistics* 13, 204–216.
- Hänelmann, S., Castelo, R., and Guinney, J. (2013). GSVA: gene set variation analysis for microarray and RNA-seq data. *BMC Bioinf.* 14, 7.
- Herrera-Galeano, J.E., Becker, D.M., Wilson, A.F., Yanek, L.R., Bray, P., Vaidya, D., Faraday, N., and Becker, L.C. (2008). A novel variant in the platelet endothelial aggregation receptor-1 gene is associated with increased platelet aggregability. *Arterioscler. Thromb. Vasc. Biol.* 28, 1484–1490.
- Hilu-Dadia, R., Hakim-Mishnaevski, K., Levy-Adam, F., and Kurant, E. (2018). Draper-mediated JNK signaling is required for glial phagocytosis of apoptotic neurons during *Drosophila* metamorphosis. *Glia* 66, 1520–1532.
- Horibata, S., Gui, G., Lack, J., DeStefano, C.B., Gottesman, M.M., and Hourigan, C.S. (2019). Heterogeneity in refractory acute myeloid leukemia. *Proc. Natl. Acad. Sci. USA* 116, 10494–10503.
- Horvath, S., and Dong, J. (2008). Geometric interpretation of gene coexpression network analysis. *PLoS Comput. Biol.* 4, e1000117.
- Horvath, S., Zhang, B., Carlson, M., Lu, K.V., Zhu, S., Felciano, R.M., Laurance, M.F., Zhao, W., Qi, S., Chen, Z., et al. (2006). Analysis of oncogenic signaling networks in glioblastoma identifies ASPM as a molecular target. *Proc. Natl. Acad. Sci. USA* 103, 17402–17407.
- Hothorn, T., Hornik, K., and Zeileis, A. (2006). Unbiased recursive partitioning: a conditional inference framework. *J. Comput. Graph Stat.* 15, 651–674.
- Huang, M.E., Ye, Y.C., Chen, S.R., Chai, J.R., Lu, J.X., Zhoa, L., Gu, L.J., and Wang, Z.Y. (1988). Use of all-trans retinoic acid in the treatment of acute promyelocytic leukemia. *Blood* 72, 567–572.
- Izzi, B., Gianfagna, F., Yang, W.Y., Cludts, K., De Curtis, A., Verhamme, P., Di Castelnuovo, A., Cerletti, C., Donati, M.B., de Gaetano, G., et al. (2019). Variation of PEAR1 DNA methylation influences platelet and leukocyte function. *Clin. Epigenetics* 11, 151.
- Izzi, B., Noro, F., Cludts, K., Freson, K., and Hoylaerts, M.F. (2018). Cell-specific PEAR1 methylation studies reveal a locus that coordinates expression of multiple genes. *Int. J. Mol. Sci.* 19, E1069.
- Izzi, B., Pistoni, M., Cludts, K., Akkor, P., Lambrechts, D., Verfaillie, C., Verhamme, P., Freson, K., and Hoylaerts, M.F. (2016). Allele-specific DNA methylation reinforces PEAR1 enhancer activity. *Blood* 128, 1003–1012.
- Jaiswal, S., Fontanillas, P., Flannick, J., Manning, A., Grauman, P.V., Mar, B.G., Lindsley, R.C., Mermel, C.H., Burtt, N., Chavez, A., et al. (2014). Age-related clonal hematopoiesis associated with adverse outcomes. *N. Engl. J. Med.* 371, 2488–2498.
- Jemal, A., Siegel, R., Xu, J., and Ward, E. (2010). Cancer statistics, 2010. *CA. Cancer J. Clin.* 60, 277–300.
- Johnson, A.D., Yanek, L.R., Chen, M.H., Faraday, N., Larson, M.G., Tofler, G., Lin, S.J., Kraja, A.T., Province, M.A., Yang, Q., et al. (2010). Genome-wide meta-analyses identifies seven loci associated with platelet aggregation in response to agonists. *Nat. Genet.* 42, 608–613.
- Jones, C.I., Bray, S., Garner, S.F., Stephens, J., de Bono, B., Angenent, W.G.J., Bentley, D., Burns, P., Coffey, A., Deloukas, P., et al. (2009). A functional genomics approach reveals novel quantitative trait loci associated with platelet signaling pathways. *Blood* 114, 1405–1416.
- Kardeby, C., Fälker, K., Haining, E.J., Criel, M., Lindkvist, M., Barroso, R., Pählsönn, P., Ljungberg, L.U., Tengdelius, M., Rainger, G.E., et al. (2019). Synthetic glycopolymers and natural fucoidans cause human platelet aggregation via PEAR1 and GPIbalpha. *Blood Adv.* 3, 275–287.
- Kauskot, A., Di Michele, M., Loyen, S., Freson, K., Verhamme, P., and Hoylaerts, M.F. (2012). A novel mechanism of sustained platelet alphallbbeta3 activation via PEAR1. *Blood* 119, 4056–4065.
- Kauskot, A., Vandebriele, C., Louwette, S., Gijsbers, R., Tousseyn, T., Freson, K., Verhamme, P., and Hoylaerts, M.F. (2013). PEAR1 attenuates megakaryopoiesis via control of the PI3K/PTEN pathway. *Blood* 121, 5208–5217.
- Keramati, A.R., Yanek, L.R., Iyer, K., Taub, M.A., Ruczinski, I., Becker, D.M., Becker, L.C., Faraday, N., and Mathias, R.A. (2019). Targeted deep sequencing of the PEAR1 locus for platelet aggregation in European and African American families. *Platelets* 30, 380–386.
- Kottaridis, P.D., Gale, R.E., Frew, M.E., Harrison, G., Langabeer, S.E., Belton, A.A., Walker, H., Wheatley, K., Bowen, D.T., Burnett, A.K., et al. (2001). The presence of a FLT3 internal tandem duplication in patients with acute myeloid leukemia (AML) adds important prognostic information to cytogenetic risk group and response to the first cycle of chemotherapy: analysis of 854 patients from the United Kingdom Medical Research Council AML 10 and 12 trials. *Blood* 98, 1752–1759.
- Krivtsov, A.V., Rozov, F.N., Zinov'yeva, M.V., Hendrikx, P.J., Jiang, Y., Visser, J.W.M., and Belyavsky, A.V. (2007). Jedi—a novel transmembrane protein expressed in early hematopoietic cells. *J. Cell. Biochem.* 101, 767–784.
- Kurtz, S.E., Eide, C.A., Kaempf, A., Khanna, V., Savage, S.L., Rofeby, A., English, I., Ho, H., Pandya, R., Bolosky, W.J., et al. (2017). Molecularly targeted drug combinations demonstrate selective effectiveness for myeloid- and lymphoid-derived hematologic malignancies. *Proc. Natl. Acad. Sci. USA* 114, E7554–E7563.

- Kuusanmäki, H., Leppä, A.M., Pölönen, P., Kontro, M., Dufva, O., Deb, D., Yadav, B., Brück, O., Kumar, A., Everaus, H., et al. (2020). Phenotype-based drug screening reveals association between venetoclax response and differentiation stage in acute myeloid leukemia. *Haematologica* **105**, 708–720.
- Lancet, J.E., Uy, G.L., Cortes, J.E., Newell, L.F., Lin, T.L., Ritchie, E.K., Stuart, R.K., Strickland, S.A., Hogge, D., Solomon, S.R., et al. (2018). CPX-351 (cytarabine and daunorubicin) liposome for injection versus conventional cytarabine plus daunorubicin in older patients with newly diagnosed secondary acute myeloid leukemia. *J. Clin. Oncol.* **36**, 2684–2692.
- Langfelder, P., and Horvath, S. (2012). Fast R functions for robust correlations and hierarchical clustering. *J. Stat. Softw.* **46**, i11.
- Langfelder, P., Zhang, B., and Horvath, S. (2008). Defining clusters from a hierarchical cluster tree: the DynamicTreeCut package for R. *Bioinformatics* **24**, 719–720.
- Lewis, J.P., Ryan, K., O'Connell, J.R., Horenstein, R.B., Damcott, C.M., Gibson, Q., Pollin, T.I., Mitchell, B.D., Beitelhees, A.L., Pakzy, R., et al. (2013). Genetic variation in PEAR1 is associated with platelet aggregation and cardiovascular outcomes. *Circ. Cardiovasc. Genet.* **6**, 184–192.
- Majumder, M.M., Leppä, A.M., Hellesøy, M., Dowling, P., Malyutina, A., Kopperud, R., Bazou, D., Andersson, E., Parsons, A., Tang, J., et al. (2020). Multi-parametric single cell evaluation defines distinct drug responses in healthy hematological cells that are retained in corresponding malignant cell types. *Haematologica* **105**, 1527–1538.
- Malani, D., Kumar, A., Brück, O., Kontro, M., Yadav, B., Hellesøy, M., Kuusanmäki, H., Dufva, O., Kankainen, M., Eldfors, S., et al. (2022). Implementing a functional precision medicine tumor board for acute myeloid leukemia. *Cancer Discov.* **12**, 388–401.
- Nanda, N., Bao, M., Lin, H., Claußer, K., Komuves, L., Quertermous, T., Conley, P.B., Phillips, D.R., and Hart, M.J. (2005). Platelet endothelial aggregation receptor 1 (PEAR1), a novel epidermal growth factor repeat-containing transmembrane receptor, participates in platelet contact-induced activation. *J. Biol. Chem.* **280**, 24680–24689.
- Ng, S.W.K., Mitchell, A., Kennedy, J.A., Chen, W.C., McLeod, J., Ibrahimova, N., Arruda, A., Popescu, A., Gupta, V., Schimmer, A.D., et al. (2016). A 17-gene stemness score for rapid determination of risk in acute leukaemia. *Nature* **540**, 433–437.
- Papaemmanuil, E., Gerstung, M., Bullinger, L., Gaidzik, V.I., Paschka, P., Roberts, N.D., Potter, N.E., Heuser, M., Thol, F., Bolli, N., et al. (2016). Genomic classification and prognosis in acute myeloid leukemia. *N. Engl. J. Med.* **374**, 2209–2221.
- Pei, S., Polley, D.A., Gustafson, A., Stevens, B.M., Minhajuddin, M., Fu, R., Riemonyd, K.A., Gillen, A.E., Sheridan, R.M., Kim, J., et al. (2020). Monocytic subclones confer resistance to venetoclax-based therapy in patients with acute myeloid leukemia. *Cancer Discov.* **10**, 536–551.
- Perl, A.E., Martinelli, G., Cortes, J.E., Neubauer, A., Berman, E., Paolini, S., Montesinos, P., Baer, M.R., Larson, R.A., Ustun, C., et al. (2019). Gilteritinib or chemotherapy for relapsed or refractory FLT3-mutated AML. *N. Engl. J. Med.* **381**, 1728–1740.
- Petersdorf, S.H., Kopecky, K.J., Slovak, M., Willman, C., Nevill, T., Brandwein, J., Larson, R.A., Erba, H.P., Stiff, P.J., Stuart, R.K., et al. (2013). A phase 3 study of gemtuzumab ozogamicin during induction and postconsolidation therapy in younger patients with acute myeloid leukemia. *Blood* **121**, 4854–4860.
- Pulte, D., Jansen, L., Castro, F.A., Krilaviciute, A., Katalinic, A., Barnes, B., Ressing, M., Holleczek, B., Luttmann, S., and Brenner, H.; GEKID Cancer Survival Working Group (2016). Survival in patients with acute myeloblastic leukemia in Germany and the United States: major differences in survival in young adults. *Int. J. Cancer* **139**, 1289–1296.
- Qayyum, R., Becker, L.C., Becker, D.M., Faraday, N., Yanek, L.R., Leal, S.M., Shaw, C., Mathias, R., Suktitipat, B., and Bray, P.F. (2015). Genome-wide association study of platelet aggregation in African Americans. *BMC Genet.* **16**, 58.
- Romine, K.A., Nechiporuk, T., Bottomly, D., Jeng, S., McWeeney, S.K., Kaempf, A., Corces, M.R., Majeti, R., and Tyner, J.W. (2021). Monocytic differ- entiation and AHR signaling as primary nodes of BET inhibitor response in acute myeloid leukemia. *Blood Cancer Discov.* **2**, 518–531.
- Scheib, J.L., Sullivan, C.S., and Carter, B.D. (2012). Jedi-1 and MEGF10 signal engulfment of apoptotic neurons through the tyrosine kinase Syk. *J. Neurosci.* **32**, 13022–13031.
- SEER (2021). National cancer Institute: surveillance, epidemiology, and end results Program. <https://seer.cancer.gov/statfacts/html/amyl.html>.
- Shen, Z.X., Chen, G.Q., Ni, J.H., Li, X.S., Xiong, S.M., Qiu, Q.Y., Zhu, J., Tang, W., Sun, G.L., Yang, K.Q., et al. (1997). Use of arsenic trioxide (As2O3) in the treatment of acute promyelocytic leukemia (APL): II. Clinical efficacy and pharmacokinetics in relapsed patients. *Blood* **89**, 3354–3360.
- Stein, E.M., DiNardo, C.D., Polley, D.A., Fathi, A.T., Roboz, G.J., Altman, J.K., Stone, R.M., DeAngelo, D.J., Levine, R.L., Flinn, I.W., et al. (2017). Enasidenib in mutant IDH2 relapsed or refractory acute myeloid leukemia. *Blood* **130**, 722–731.
- Stone, R.M., Mandrekar, S.J., Sanford, B.L., Laumann, K., Geyer, S., Bloomfield, C.D., Thiede, C., Prior, T.W., Döhner, K., Marcucci, G., et al. (2017). Midostaurin plus chemotherapy for acute myeloid leukemia with a FLT3 mutation. *N. Engl. J. Med.* **377**, 454–464.
- Storey, J.D., and Tibshirani, R. (2003). Statistical significance for genomewide studies. *Proc. Natl. Acad. Sci. USA* **100**, 9440–9445.
- Strobl, C., Boulesteix, A.L., Zeileis, A., and Hothorn, T. (2007). Bias in random forest variable importance measures: illustrations, sources and a solution. *BMC Bioinf.* **8**, 25.
- Sullivan, C.S., Scheib, J.L., Ma, Z., Dang, R.P., Schafer, J.M., Hickman, F.E., Brodsky, F.M., Ravichandran, K.S., and Carter, B.D. (2014). The adaptor protein GULP promotes Jedi-1-mediated phagocytosis through a clathrin-dependent mechanism. *Mol. Biol. Cell* **25**, 1925–1936.
- Sun, Y., Vandenbriele, C., Kauskot, A., Verhamme, P., Hoylaerts, M.F., and Wright, G.J. (2015). A human platelet receptor protein microarray identifies the high affinity immunoglobulin E receptor subunit alpha (FcεRIα) as an activating platelet endothelium aggregation receptor 1 (PEAR1) ligand. *Mol. Cell. Proteomics* **14**, 1265–1274.
- Tomfohr, J., Lu, J., and Kepler, T.B. (2005). Pathway level analysis of gene expression using singular value decomposition. *BMC Bioinf.* **6**, 225.
- Tyner, J.W., Tognon, C.E., Bottomly, D., Wilmot, B., Kurtz, S.E., Savage, S.L., Long, N., Schultz, A.R., Traer, E., Abel, M., et al. (2018). Functional genomic landscape of acute myeloid leukaemia. *Nature* **562**, 526–531.
- Van Galen, P., Hovestadt, V., Wadsworth Li, M.H., Hughes, T.K., Griffin, G.K., Battaglia, S., Verga, J.A., Stephansky, J., Pastika, T.J., Lombardi Story, J., et al. (2019). Single-cell RNA-seq reveals AML hierarchies relevant to disease progression and immunity. *Cell* **176**, 1265–1281.e24.
- Vandenbriele, C., Kauskot, A., Vandersmissen, I., Criel, M., Geenens, R., Craps, S., Luttmann, A., Janssens, S., Hoylaerts, M.F., and Verhamme, P. (2015). Platelet endothelial aggregation receptor-1: a novel modifier of neangiogenesis. *Cardiovasc. Res.* **108**, 124–138.
- Vandenbriele, C., Sun, Y., Criel, M., Cludts, K., Van Kerckhoven, S., Izzi, B., Vanassche, T., Verhamme, P., and Hoylaerts, M.F. (2016). Dextran sulfate triggers platelet aggregation via direct activation of PEAR1. *Platelets* **27**, 365–372.
- Wang, Y.H., Lin, C.C., Yao, C.Y., Hsu, C.L., Hou, H.A., Tsai, C.H., Chou, W.C., and Tien, H.F. (2020). A 4-gene leukemic stem cell score can independently predict the prognosis of myelodysplastic syndrome patients. *Blood Adv.* **4**, 644–654.
- White, B.S., Khan, S.A., Mason, M.J., Ammad-Ud-Din, M., Potdar, S., Malani, D., Kuusamäki, H., Druker, B.J., Heckman, C., Kallioniemi, O., et al. (2021). Bayesian multi-source regression and monocyte-associated gene expression predict BCL-2 inhibitor resistance in acute myeloid leukemia. *NPJ Precis. Oncol.* **5**, 71.
- Wu, H.H., Bellmunt, E., Scheib, J.L., Venegas, V., Burkert, C., Reichardt, L.F., Zhou, Z., Fariñas, I., and Carter, B.D. (2009). Glial precursors clear sensory neuron corpses during development via Jedi-1, an engulfment receptor. *Nat. Neurosci.* **12**, 1534–1541.

Zhan, Q., Ma, X., and He, Z. (2020). PEAR1 suppresses the proliferation of pulmonary microvascular endothelial cells via PI3K/AKT pathway in ALI model. *Microvasc. Res.* **128**, 103941.

Zhang, B., and Horvath, S. (2005). A general framework for weighted gene co-expression network analysis. *Stat. Appl. Genet. Mol. Biol.* **4**, Article17.

Zhang, H., Nakauchi, Y., Köhnke, T., Stafford, M., Bottomly, D., Thomas, R., Wilmot, B., McWeeney, S.K., Majeti, R., and Tyner, J.W. (2020). Integrated analysis of patient samples identifies biomarkers for venetoclax efficacy and combination strategies in acute myeloid leukemia. *Nat. Cancer* **1**, 826–839.

## STAR★METHODS

### KEY RESOURCES TABLE

REAGENT or RESOURCE	SOURCE	IDENTIFIER
<b>Antibodies</b>		
BV650 Mouse Anti-Human PEAR1, clone 492621	BD Biosciences	Catalog # 748063; RRID: AB_2872524
Human TruStain FcX (Fc Receptor Blocking Solution)	Biolegend	Catalog # 422301; RRID: AB_2818986
<b>Biological samples</b>		
AML Patient Samples	Oregon Health & Science University (OHSU), University of Utah, University of Texas Medical Center (UT Southwestern), Stanford University, University of Miami, University of Colorado, University of Florida, National Institutes of Health (NIH), Fox Chase Cancer Center and University of Kansas (KUMC)	OHSU; IRB#9570; #4422; NCT01728402
Healthy Bone Marrow CD34 <sup>+</sup> Cells	AllCells	Custom Order
<b>Chemicals, peptides, and recombinant proteins</b>		
Drug	Source	Catalog #   CAS #
17-AAG (Tanespimycin)	LC Labs	A-6880   75747-14-7
A-674563	Selleck	S2670   552325-73-2
ABT-737	Selleck	S1002   852808-04-9
Afatinib (BIBW-2992)	LC Labs	A-8644   850140-72-6
AGI-5198	Selleck	S7185   1355326-35-0
AGI-6780	Selleck	S7241   1432660-47-3
AKT Inhibitor IV	Millipore Sigma (EMD Biosciences; Calbiochem)	124011   681281-88-9
AKT Inhibitor X	Millipore Sigma (EMD Biosciences; Calbiochem)	124020   925681-41-0
Alisertib (MLN8237)	Selleck	S1133   1028486-01-2
AMPK Inhibitor	Millipore Sigma (EMD Biosciences; Calbiochem)	171260   866405-64-3
Arsenic trioxide	Fisher	NC0244675   1327-53-3
Artemisinin	Selleck	S1282   63968-64-9
AST487	Selleck	S6662   630124-46-8
AT-101	Selleck	S2812   866541-93-7
AT7519	Selleck	S1524   844442-38-2
Axitinib (AG-013736)	LC Labs	A-1107   319460-85-0
Azacytidine	Selleck	S1782   320-67-2
AZD1480	Selleck	S2162   935666-88-9
Baicalein	Selleck	S2268   491-67-8
Barasertib (AZD1152-HQPA)	Selleck	S1147   722544-51-6
Bay 11-7085	Selleck	S7352   196309-76-9
BEZ235	LC Labs	N-4288   915019-65-7
BI-2536	Selleck	S1109   755038-02-9
Birinapant	Selleck	S7015   1260251-31-7
BLZ945	Selleck	S7725   953769-46-5
BMS-345541	Selleck	S8044   445430-58-0
BMS-754807	Selleck	S1124   1001350-96-4

(Continued on next page)

**Continued**

REAGENT or RESOURCE	SOURCE	IDENTIFIER
Bortezomib (Velcade)	LC Labs	B-1408   179324-69-7
Bosutinib (SKI-606)	LC Labs	B-1788   380843-75-4
Cabozantinib (XL184)	Selleck	S1119   849217-68-1
Canertinib (CI-1033)	LC Labs	C-1201   289499-45-2
Cediranib (AZD2171)	LC Labs	C-4300   288383-20-0
CHIR-99021	LC Labs	C-6556   252917-06-9
CI-1040 (PD184352)	LC Labs	P-8499   212631-79-3
Crenolanib	Selleck	S2730   670220-88-9
Crizotinib (PF-2341066)	LC Labs	C-7900   877399-52-5
CYT387	Selleck	S2219   1056634-68-4
Cytarabine	Selleck	S1648   147-94-4
Dasatinib	LC Labs	D-3307   302962-49-8
DBZ	Tocris	4489   209984-56-5
Doramapimod (BIRB 796)	LC Labs	D-2744   285983-48-4
Dovitinib (CHIR-258)	LC Labs	D-3608   405169-16-6
Elesclomol	Selleck	S1052   488832-69-5
Entospletinib (GS-9973)	Selleck	S7523   1229208-44-9
Entrectinib	Selleck	S7998   1108743-60-7
Erlotinib	LC Labs	E-4007   183319-69-9
Etomoxir	Selleck	S8244   828934-41-4
Everolimus	Selleck	S1120   159351-69-6
Flavopiridol	Selleck	S1230   131740-09-5
Foretinib (XL880)	LC Labs	F-4185   849217-64-7
GDC-0879	Selleck	S1104   905281-76-7
GDC-0941	LC Labs	G-9252   957054-30-7
Gefitinib	LC Labs	G-4408   84475-35-2
Gilteritinib	Selleck	S7754   1254053-43-4
Go6976	LC Labs	G-6203   136194-77-9
GSK-2879552	Selleck	S7796   1902123-72-1
GSK690693	Selleck	S1113   937174-76-0
GW-2580	LC Labs	G-5903   870483-87-7
H-89	LC Labs	H5239   127243-85-0
Ibrutinib (PCI-32765)	LC Labs	I-3311   936563-96-1]
Idelalisib (GS-1101)	Selleck	S2226   870281-82-6
Imatinib	LC Labs	I5577   152459-95-5
Indisulam	Selleck	S9742   165668-41-7
INK-128	Selleck	S2811   1224844-38-5
JAK Inhibitor I	Millipore Sigma (EMD Biosciences; Calbiochem)	420099   457081-03-7
JNJ-28312141	SYN Kinase	SYN-1154   885692-52-4
JNJ-38877605	Selleck	S1114   943540-75-8
JNJ-7706621	Selleck	S1249   443797-96-4
JNK Inhibitor II (SP600126)	LC Labs	S-7979   129-56-6
JQ1	Selleck	S7110   1268524-70-4
KI20227	Tocris	4481   623142-96-1
KN92	Tocris	4130   1135280-28-2
KN93	Tocris	1278   139298-40-1
KU-55933	Selleck	S1092   587871-26-9
KW-2449	Selleck	S2158   1000669-72-6

(Continued on next page)

**Continued**

REAGENT or RESOURCE	SOURCE	IDENTIFIER
Lapatinib	Selleck	S2111   231277-92-2
Lenalidomide	Selleck	S1029   191732-72-6
Lenvatinib	Selleck	S1164   857890-39-2
Lestaurtinib (CEP-701)	LC Labs	L-6307   111358-88-4
Linifanib (ABT-869)	Selleck	S1003   796967-16-3
Lovastatin	Selleck	S2061   75330-75-5
LY-333531	Tocris	4738   169939-93-9
LY294002	LC Labs	L-7962   154447-36-6
Masitinib (AB-1010)	LC Labs	M-7007   790299-79-5
MEK Inhibitor VII	Millipore Sigma (EMD Biosciences; Calbiochem)	444939   305350-87-2
Metformin	Selleck	S5958   657-24-9
MGCD-265	Selleck	S1361   875337-44-3
Midostaurin	LC Labs	P-7600   120685-11-2
MK-2206	Selleck	S1078   1032350-13-2
MLN120B	MedChem Express	HY-15473   783348-36-7
MLN8054	Selleck	S1100   869363-13-3
Motesanib (AMG-706)	LC Labs	M-2900   857876-30-3
Neratinib (HKI-272)	Selleck	S2150   698387-09-6
NF-κB Activation Inhibitor	Selleck	S4902   545380-34-5
Nilotinib	Selleck	S1033   641571-10-0
Nutlin 3a	Selleck	S8059   675576-98-4
NVP-ADW742	Selleck	S1088   475488-23-4
NVP-AEW541	Selleck	S1034   475489-16-8
NVP-TAE684	Selleck	S1108   761439-42-3
Olaparib	Selleck	S1060   763113-22-0
OTX-015	Selleck	S7360   202590-98-5
p38 MAP Kinase Inhibitor	Millipore Sigma (EMD Biosciences; Calbiochem)	506126   219138-24-6
Palbociclib	Selleck	S4482   571190-30-2
Panobinostat	Selleck	S1030   404950-80-7
Pazopanib (GW786034)	LC Labs	P6706   444731-52-6
PD153035	Millipore Sigma (EMD Biosciences; Calbiochem)	SML0564   183322-45-4
PD173955	Symanis	SY-PD173955   260415-63-2
PD98059	LC Labs	P-4313   167869-21-8
Pelitinib (EKB-569)	Selleck	S1392   257933-82-7
Perhexiline maleate	Selleck	S6959   6724-53-4
PH-797804	Selleck	S2726   586379-66-0
PHA-665752	Selleck	S1070   477575-56-7
PHT-427	Selleck	S1556   1191951-57-1
PI-103	Selleck	S1038   371935-74-9
PLX-4720	Selleck	S1152   918505-84-7
Ponatinib (AP24534)	LC Labs	P-7022   943319-70-8
PP2	Millipore Sigma (EMD Biosciences; Calbiochem)	529573   172889-27-9
PP242	LC Labs	P-6666   1092351-67-1
PRT062070 HCL	Selleck	S7634   1369761-01-2
PRT062607	Selleck	S8032   1370261-97-4

(Continued on next page)

**Continued**

REAGENT or RESOURCE	SOURCE	IDENTIFIER
Quizartinib (AC220)	LC Labs	Q-4747   950769-58-1
R406	Selleck	S2194   841290-81-1
R547	Selleck	S2688   741713-40-6
RAF265 (CHIR-265)	Selleck	S2161   927880-90-8
Ralimetinib (LY2228820)	Selleck	S1494   862507-23-1
Ranolazine (free base)	Selleck	S1799   95635-55-5
Rapamycin	LC Labs	R-5000   53123-88-9
Regorafenib (BAY 73-4506)	Selleck	S1178   755037-03-7
Roscovitine (CYC-202)	LC Labs	R-1234   186692-46-6
Ruxolitinib, free base	LC Labs	R-6600   120685-11-2
S31-201	Santa Cruz Biotech	sc-204304   501919-59-1
Saracatinib (AZD0530)	LC Labs	S-8906   379231-04-6
SB-202190	LC Labs	S-1700   152121-30-7
SB-203580	LC Labs	S-3400   152121-47-6
SB-431542	Selleck	S1067   301836-41-9
Selinexor	Selleck	S7252   1393477-72-9
Selumetinib (AZD6244)	LC Labs	S-4490   606143-52-6
SGX-523	Selleck	S1112   1022150-57-7
SNS-032 (BMS-387032)	Selleck	S1145   345627-80-7
Sorafenib tosylate	LC Labs	S-8502   475207-59-1
SR9011-HCL	MedChem Express	HY-16988A   2070014-94-5
Staurosporine, free base	LC Labs	S-9300   62996-74-1]
STO609	Millipore Sigma (EMD Biosciences; Calbiochem)	570250   52029-86-4
SU11274	Selleck	S1080   658084-23-2
SU14813	Selleck	S0504   627908-92-3
Sunitinib malate	LC Labs	S-8803   341031-54-7
SYK Inhibitor	Millipore Sigma (EMD Biosciences; Calbiochem)	574711   622387-85-3
Tandutinib (MLN518)	LC Labs	T-7802   387867-13-2
TG100-115	Selleck	S1358   677297-51-7
TG101348	Active Biochem	A-1140   936091-26-8
Tivozanib (AV-951)	LC Labs	T-6466   475108-18-0
Tofacitinib (CP-690550)	LC Labs	T-1377   477600-75-2
Tozastertib (VX-680)	LC Labs	T-2304   639089-54-6
Trametinib (GSK1120212)	LC Labs	T-8132   871700-17-3
Vandetanib (ZD6474)	LC Labs	V-9402   443913-73-3
Vargeteaf (Nintedanib)	LC Labs	N-9077   656247-17-5
Vatalanib (PTK787)	LC Labs	V-8303   212141-51-0
Vemurafenib (PLX4032)	LC Labs	V-2800   918504-65-1
Venetoclax	LC Labs	V-3579   1257044-40-8
Vismodegib (GDC-0449)	LC Labs	V-4050   879085-55-9
Volasertib (BI-6727)	Selleck	S2235   755038-65-4
VX-745	Tocris	3915   209410-46-8
XAV-939	Selleck	S1180   284028-89-3
XMD 8-87	Selleck	S8272   1234480-46-6
YM-155	Selleck	S1130   781661-94-7
Other Chemical	Source	Catalog #
Zombie Aqua Fixable Viability Dye	Biolegend	Catalog # 423101

(Continued on next page)

**Continued**

REAGENT or RESOURCE	SOURCE	IDENTIFIER
<b>Critical commercial assays</b>		
Nextera RapidCapture Exome	Illumina	
SureSelect Strand-Specific RNA Library Preparation Kit	Agilent	
DNeasy Blood & Tissue Kit	Qiagen	
RNeasy Mini Kit	Qiagen	
<b>Deposited data</b>		
DNA Sequencing Data	This paper	<a href="https://vizome.org/aml2">vizome.org/aml2</a> , dbGaP study ID is 30641 and accession ID is phs001657.v2.p1
RNA Sequencing Data	This paper	<a href="https://vizome.org/aml2">vizome.org/aml2</a> , dbGaP study ID is 30641 and accession ID is phs001657.v2.p1
<b>Oligonucleotides</b>		
Custom capture probes for DNA sequencing (11.9 MB)	Roche-Nimblegen	Sequencing coordinates listed Table S14 of ( <a href="#">Tyner et al., 2018</a> )
Forward Primer <i>FLT3</i> : 5'- AGCA ATT TAG GTA TGA AAG CCA GCTA -3'	Eurofins	( <a href="#">Kottaridis et al., 2001</a> )
Reverse Primer <i>FLT3</i> : 5'-CTT TCA GCA TTT TGA CGG CAA CC -3'	Eurofins	( <a href="#">Kottaridis et al., 2001</a> )
Forward Primer <i>NPM1</i> : 5'-GTT TCT TTT TTT TTT CCA GGC TAT TCA AG -3'	Eurofins	( <a href="#">Falini et al., 2007</a> )
Reverse Primer <i>NPM1</i> : 5'-CAC GGT AGG GAA AGT TCT CAC TCT GC -3'	Eurofins	( <a href="#">Falini et al., 2007</a> )
<b>Software and algorithms</b>		
R version 4.03	R Core Team	<a href="https://www.r-project.org">https://www.r-project.org</a>
R package GSVA v1.38	Bioconductor	<a href="https://doi.org/10.18129/B9.bioc.GSVA">https://doi.org/10.18129/B9.bioc.GSVA</a>
R package cqn v1.36	Bioconductor	<a href="https://doi.org/10.18129/B9.bioc.cqn">https://doi.org/10.18129/B9.bioc.cqn</a>
R package qvalue v2.22.0	Bioconductor	<a href="https://doi.org/10.18129/B9.bioc.qvalue">https://doi.org/10.18129/B9.bioc.qvalue</a>
R package partykit v1.2-15	CRAN	<a href="https://CRAN.R-project.org/package=partykit">https://CRAN.R-project.org/package=partykit</a>
R package survival v3.2-7	CRAN	<a href="https://CRAN.R-project.org/package=survival">https://CRAN.R-project.org/package=survival</a>
R package WGCNA v1.69	CRAN	<a href="https://CRAN.R-project.org/package=WGCNA">https://CRAN.R-project.org/package=WGCNA</a>
R package data.table v1.13.6	CRAN	<a href="https://CRAN.R-project.org/package=data.table">https://CRAN.R-project.org/package=data.table</a>
Manuscript analysis workflow	This paper	<a href="https://doi.org/10.5281/zenodo.6773715">https://doi.org/10.5281/zenodo.6773715</a>
<b>Other</b>		
Ex Vivo Drug Sensitivity Data	This paper	<a href="https://vizome.org/aml2">vizome.org/aml2</a> and <a href="https://biodev.github.io/BeatAML2/">https://biodev.github.io/BeatAML2/</a>
Clinical Annotations	This paper	Table S1

## RESOURCE AVAILABILITY

### Lead contact

Further information and requests for resources and reagents should be directed to and will be fulfilled by the lead contact, Dr. Jeffrey Tyner ([tynerj@ohsu.edu](mailto:tynerj@ohsu.edu)).

### Materials availability

This study did not generate unique reagents.

## Data and code availability

All raw and processed sequencing data, along with relevant clinical annotations have been submitted to dbGaP and Genomic Data Commons and are publicly available. The dbGaP study ID is 30641 and accession ID is phs001657.v2.p1 ([https://www.ncbi.nlm.nih.gov/projects/gap/cgi-bin/study.cgi?study\\_id=phs001657.v2.p1](https://www.ncbi.nlm.nih.gov/projects/gap/cgi-bin/study.cgi?study_id=phs001657.v2.p1)). The clinical annotations and data availability are found in Table S1. In addition, all data can be accessed and queried through our online, interactive user interface, Vizome, at [vizome.org/aml2](https://vizome.org/aml2). Original code for replicating the paper analyses based on publicly available data has been deposited at [https://github.com/biodev/beataml2\\_manuscript](https://github.com/biodev/beataml2_manuscript). The DOI is listed in the [key resources table](#). A frequently asked questions page for the dataset is found at <https://biodev.github.io/BeatAML2/>.

## EXPERIMENTAL MODEL AND SUBJECT DETAILS

### Patient sample collection and cohort organization

The complete Oregon Health & Science University (OHSU) Beat AML cohort represents sample collection and characterization over a span of 10 years. The initial cohort, first reported in (Tyner et al., 2018) represent the first two waves of patient accrual and sample data (denoted “Waves 1 + 2”). Additional longitudinal samples for Waves 1 + 2, in addition to patient accrual represents the final two waves (“Waves 3 + 4”). Harmonization of these datasets together for specific analyses is denoted as the “harmonized data”. For this manuscript we only utilized specimens from the first available timepoint (defined by a 5-day interval) for each patient such that each patient was represented by a single sample for a given datatype. Additionally, we removed samples taken while a patient was in remission from consideration.

All patients gave informed consent to participate in this study, which had the approval and guidance of the institutional review boards at OHSU, University of Utah, University of Texas Medical Center (UTSW), University of Miami, University of Colorado, University of Florida, National Institutes of Health (NIH), and University of Kansas (KUMC). Samples were sent to the coordinating center (OHSU; IRB#9570; #4422; NCT01728402) where they were coded and processed. Specific names of centers associated with each specimen were coded and centers providing less than 5 samples were aggregated together and given one center identifier. Clinical, prognostic, genetic, cytogenetic, and pathologic lab values as well as treatment and outcome data were manually curated from patient electronic medical records. Patients were assigned a specific diagnosis based on the prioritization of genetic and clinical factors as determined by WHO guidelines (Arber et al., 2016). To prevent re-identification, any patient over the age of 90 was placed into a >90 aggregated age bracket. Genetic characterization of the leukemia samples included results of clinical deep-sequencing panels of genes commonly mutated in hematologic malignancies (Sequenom and GeneTrails (OHSU); Foundation Medicine (UTSW); Genoptix; and Illumina).

## METHOD DETAILS

### Patient specimen processing

Processing of patient specimens, isolation of nucleic acids, DNA- and RNA-sequencing, detection of FLT3-ITD and 4-base pair NPM1 insertion, performance of ex vivo drug sensitivity assays, and initial analytical workflows were performed in identical fashion as in our prior study (Tyner et al., 2018). Any changes that were made to analytical approaches and techniques employed in this study are described below.

### DNA sequencing

For DNA sequencing, we used the 11.9 megabase custom capture library that was developed to provide coverage of all variants previously reported in AML (including all variants that were detected from exome sequencing in our prior study). The genes, variants, and capture regions for this custom library were reported in the [supplemental information](#) of our prior study (Table S14 in (Tyner et al., 2018)), as well as detailed methods for pre-processing and analysis ([STAR Methods](#)).

### European leukemia network prognostic categorization

Some updates were implemented to our pipeline for calling ELN categories. First, we confined calls in this study to specimens taken at initial acute leukemia diagnosis, and did not place specimens that were taken in remission, at relapse, or from cases with a non-AML diagnosis (e.g. MDS) into ELN categories. Second, for consideration of mutation of ASXL1, RUNX1, or TP53, we used our internal deep sequencing data as the primary source of information, rather than clinical sequencing results curated from the electronic medical record. This was due to a higher percentage of samples with available sequencing data for these three genes from our internal versus curated clinical data. We compared our internal results with available clinical sequencing results for these genes, and we manually adjudicated the minority of instances where discrepancies existed. We also manually adjudicated calls for biallelic CEBPA, using both our internal sequencing and results from clinical sequencing. Relevant cytogenetic events were parsed from clinical karyotype and cytogenetic results, and we used our consensus FLT3-ITD and NPM1 calls as described in our prior study (Tyner et al., 2018), including data from internal PCR amplicon size-based evaluation using published primers (Falini et al., 2007; Kottaridis et al., 2001). All of these results were used to call Favorable, Intermediate, or Adverse categories according to the ELN 2017 criteria established in (Dohner et al., 2017) with a minority of cases requiring indication of uncertainty due to lack of knowledge regarding FLT3-ITD allelic ratio. Finally, we discontinued usage of calls based on the 2008 ELN guidelines.

**Ex vivo functional drug Screen data processing**

Dose-response curves for all the drugs were fit using probit models ([Kurtz et al., 2017](#)) similar to the flagship Beat AML manuscript ([Tyner et al., 2018](#)). However, the QC and summarization approach was modified for the situations where multiple replicates were available. In the description below, a profile indicates a sample - inhibitor pair. Profiles with no replicates were subject to probit curve fit thresholds. Specifically, profiles with both Deviance >2 and AIC >12 were removed. Profiles with replicates were first assessed based on the variability of the readouts (normalized viability capped at 100%). For each plate, the standard deviation (SD) across replicates for each of the 7 concentration points was assessed and the plate was removed if 4 or more of the concentrations were considered highly variable (SD > 25). If replicates were available across multiple plates, the viability at each concentration point was first averaged per plate. The SD across plates was computed per concentration point similar to above and an AUC was computed from probit fits to each plate. Similar to the initial replicate filter, profiles were removed if both four or more concentrations had highly variable SD and the SD(AUC) > 50. Finally, a single probit curve was used to determine the AUC and IC values for each profile. As with ([Tyner et al., 2018](#)), drug response is indicated by color coding scheme (i.e., Red – sensitivity, white - intermediate, Blue - resistance).

**Organization of drugs into families based on targets and pathways**

We utilized two primary data sources for information regarding drug/target relationships, Targetome ([Blucher et al., 2017, 2019](#); [Choonoo et al., 2019](#)) and KINOMEscan ([Davis et al., 2011](#)). For determination of top tier targets of each drug from KINOMEscan and Targetome V2 data, we used a threshold that was 10-fold higher than the second lowest Kd for each drug (termed Tier1 hits). We defined a set of high confidence drug/target relationships requiring either a Tier1 with at most a Kd of 25 in KINOMEscan and/or Targetome. Additionally, we required Targetome to have at least two references with at least two unique supporting assay values. This high confidence set was combined with a small number of additional interactions annotated manually (see [Table S4](#) for full annotations of drug family targets). We utilized the International Union of Basic and Clinical Pharmacology (IUPHAR) family classifications for targets ([Armstrong et al., 2020](#)). Targets were assigned to the lowest level of the family hierarchy as well as up to two higher levels. The resulting inhibitor/family relationships were additionally manually curated.

**Inhibitor family response**

To generate gene family scores, we first rescaled the inhibitor AUC responses to be between 0 and 1 in order to ensure comparability between inhibitors with different concentration ranges. We then used the single sample gene set enrichment analysis (GSEA) (ssGSEA ([Barbie et al., 2009](#))) approach as implemented in gene set variation analysis (GSVA) package ([Hanzelmann et al., 2013](#)) to generate a score per family. We required at least 5 inhibitors per family and did not implement the cohort range normalization as only a single patient was provided at a time. Note that the use of ssGSEA as opposed to a principal component-based scoring was driven by the need to account for differences in drug coverage amongst patients.

**RNA sequencing**

Gene-level RNASeq counts were generated as in the previous Beat AML manuscript ([Tyner et al., 2018](#)). Again, we used conditional quantile normalization (CQN ([Hansen et al., 2012](#))). In order to facilitate comparison with previous results we used the CQN reference distribution parameters learned from the Waves 1 + 2 samples to apply the normalization to the Waves 3 + 4 samples.

**Weighted gene Co-expression network analysis****Module formation and summarization**

We started with the original set of 14 gene expression modules (13 + Mod0 (gray) ‘outlier’ module) from the Beat AML manuscript derived using the weighted gene co-expression network analysis (WGCNA) ([Zhang and Horvath, 2005](#)) methodology. With the exception of Mod0 (gray), these gene sets are typically summarized by their ‘eigengene’ which is their first principal component (PC) score ([Horvath and Dong, 2008](#)). As the mod0 (gray) gene-set was more heterogeneous, we kept the first 5 PC scores for the eigengene. Since the CQN normalization approach above did not change the original data, we were able to directly ‘predict’ the PC scores of the Waves 3 + 4 cohort for each module. First, we centered and scaled (C/S) the Waves 3 + 4 cohort expression matrix using the mean and standard deviations estimated from the original cohort. We then formed scores per Waves 3 + 4 cohort patient as the linear combination of their C/S expression values and the corresponding column of the original matrix of eigenvectors/rotations.

**Module membership**

A standard WGCNA methodology is the formation of kME values which are defined as the correlation of gene expression with the module eigengene (PC1 score as described above) ([Langfelder et al., 2008](#)). Genes with high kME are considered to have higher (fuzzy) membership in each module or alternatively can be seen as more ‘hub-like’ in a network context ([Horvath and Dong, 2008](#)). In this instance the correlation used was the robust biweight midcorrelation ([Langfelder and Horvath, 2012](#)).

**Module associations**

To relate WGCNA modules to external continuous variables, we assessed direct correlation of a variable with a module eigengene which indicates whether the pattern of a module covaries with the variable ([Horvath et al., 2006](#)).

### Cell-type scores

We first divided the Waves 1 + 2 cohort with RNASeq samples by whether they were bone marrow derived or from peripheral blood/leukapheresis and centered and scaled them separately. Using the top 30 genes for each of six single-cell AML tumor-derived signatures (Van Galen et al., 2019), we computed gene set scores. Similar to the WGCNA eigengenes, our scores were based on the first principal component and aligned with the average expression. This is similar to the approach used in the context of pathway-based geneset analysis (PLAGE (Tomfohr et al., 2005)). Waves 3 + 4 cell-type scores were ‘predicted’ from ‘Waves 1 + 2’ using the same approach described for the WGCNA eigengenes but this time using separate centering and scaling for the specimen types.

### Formation of genomic features

We first combined the set of expression module and cell-type scores from the RNASeq samples. The two continuous datatypes were correlated, often with modules having opposing correlations with cell-types associated with low and high differentiation. To address this, we removed the expression modules seen as being both positively and negatively correlated ( $\text{abs}(r) \geq 0.6$ ) with a cell-type. The consensus AML fusions and mutation calls were then added in as binary features.

### Random survival forest

Using the combined set of genomic features, we fit a conditional random forest (cforest) model using the ‘partykit’ package with post-diagnosis survival, measured in days, as the outcome (Hothorn et al., 2006). Our model utilized 1,000 trees and 63.2% subsampling as opposed to the bootstrap as previously suggested (Strobl et al., 2007). We used the predictions (i.e.  $\log_{10}$  median survival) from this ‘model to fit a single surrogate conditional inference tree model to facilitate interpretation (Pearson’s correlation between model predictions: 0.877).

Where indicated, high vs low group categorizations were also performed using ctree but limiting depth to a single split and requiring minimum group size of 20.

### LSC17

For comparisons with the LSC17 signature (Ng et al., 2016), we replicated the signature using the coefficients in the manuscript, which was reported as the optimized signature by the authors (which was also patented WO2017132749A1). Categorization of expression for Hazard Ratio and other analyses was done using two different “split types”: median as described in (Ng et al., 2016) or ctree to facilitate comparison with PEAR1.

### Clinical curation via natural language processing (NLP)

A natural language processing (NLP) workflow was developed to automatically extract key clinical data elements that were only available in the Electronic Health Records (EHR) in unstructured clinical notes. The NLP pipeline was written in Python which incorporated a commercially available text miner - Linguamatics’ Interactive Information Extraction (I2E) platform, as a major component, along with Python-based document pre-processing, results output logic, and evaluation components. Data from the manually curated Gold Standard DataSet (GSDS) from Waves 1 + 2 were used to evaluate the performance of the NLP system. An NLP DataSet (NLPDS) was assembled that contained as far as possible the source pathology documents set from which the GSDS was originally obtained by manual review supervised by the data manager. This was subdivided into five partitions, and used in an iterative training-development-validation cycle to optimize the NLP and Python code. For evaluation purposes, we treated partitions 1 and 2 as a single training set and partitions 3, 4, and 5 as a single test set. Overall, the training set consisted of 108 patients with 134 specimens and 241 documents, and the test set consisted of 252 patients with 289 specimens and 532 documents. Evaluation of NLP results led in some cases to discovery of missing or incorrect data in the GSDS (which was estimated to have an overall error rate of 9%), further improving data quality. For the NLP data by data element, Accuracy ranged from 79% to 93%, Precision 85%–96%, Recall from 76% to 93% and F1-score (the harmonic mean of the precision and recall) 81%–94%.

### PEAR1 flow cytometry analysis

AML patient samples were thawed, washed in pre-warmed media, and resuspended in PBS (PBS). Cells were then stained for viability via zombie aqua dye (Biolegend, #423101) for 15 min. Cells were washed in FACS buffer (PBS, 2% fetal bovine serum, sodium azide, EDTA) and then Fc receptors were blocked for 5 min (Biolegend, #422301) prior to staining with anti-PEAR1 antibody conjugated to brilliant violet 650 (clone 492,621; BD Biosciences Catalog #748063) at a dilution of 1:40 for 30 min covered on ice. Cells were then fixed with 2% paraformaldehyde for 20 min and analyzed with a Cytek Aurora flow cytometer. Analysis and figure generation was performed with FlowJo Software. PEAR1 positive cells were identified by first gating single cells using forward and side scatter, then gating only live cells (zombie aqua dye negative), then gating for PEAR1+ cells as compared to a fluorescence minus one (FMO) control.

### QUANTIFICATION AND STATISTICAL ANALYSIS

In all cases, statistical analyses of data, including tests used, exact value of n (where n indicates the number of patient specimens that were available for a given analysis), definition of center, dispersion, and precision measures, and correction for false discovery rate (FDR) are reported in the descriptive sections of the results, [Method details](#) section of [STAR Methods](#), in corresponding figure

legends, and in figures, themselves, where possible. Measures of significance or correlation are reported as p- or r-values, with p values corrected for FDR, where appropriate. All patient specimens with material sufficient for analysis and with data passing quality control thresholds (described above in [Method details](#) section of [STAR Methods](#) and in ([Tyner et al., 2018](#))) were included in the cohort and dataset.

#### ADDITIONAL RESOURCES

All data can be accessed and queried through our online, interactive user interface, Vizome, at [vizome.org/aml2](#). Original code for replicating the paper analyses based on publicly available data has been deposited at [https://github.com/biodev/beataml2\\_manuscript](https://github.com/biodev/beataml2_manuscript). The digital object identifier (DOI) is listed in the [key resources table](#). A frequently asked questions PAGE for the dataset is found at <https://biodev.github.io/BeatAML2/>.